**SURFACE CHEMISTRY MANIPULATION OF GOLD
NANORODS DISPLAYS HIGH CELLULAR UPTAKE
IN VITRO WHILE PRESERVING OPTICAL PROPERTIES
FOR BIO-IMAGING AND PHOTO-THERMAL APPLICATIONS**

ANTHONY B. POLITO III, Maj, USAF, BSC, PhD, MT(ASCP)SBB
March 2016
Final Report for March 2015 to DEC 2015

REPORT DOCUMENTATION PAGE

Form Approved
OMB No. 0704-0188

1. REPORT DATE *(DD-MM-YYYY)* 28-03-2016	2. REPORT TYPE Final	3. DATES COVERED *(From - To)* 7/2012 –1/2016

4. TITLE AND SUBTITLE

SURFACE CHEMISTRY MANIPULATION OF GOLD NANORODS DISPLAYS HIGH CELLULAR UPTAKE IN VITRO WHILE PRESERVING OPTICAL PROPERTIES FOR BIO-IMAGING AND PHOTO-THERMAL APPLICATIONS.

5a. CONTRACT NUMBER

5b. GRANT NUMBER

5c. PROGRAM ELEMENT NUMBER

6. AUTHOR(S)
ANTHONY B. POLITO III, Maj, USAF, BSC, PhD, MT(ASCP)SBB

5d. PROJECT NUMBER

5e. TASK NUMBER

5f. WORK UNIT NUMBER

7. PERFORMING ORGANIZATION NAME(S) AND ADDRESS(ES)
Air Force Institute of Technology (AFIT) Civilian Institution Programs (CIP)
2950 Hobson Way
WPAFB OH 45433-7765

8. PERFORMING ORGANIZATION REPORT NUMBER

9. SPONSORING/MONITORING AGENCY NAME(S) AND ADDRESS(ES)
Clinical Investigations
Office of the Air Force Surgeon General SG5M,
Research and Innovations
7700 Arlington Blvd, Ste 5164
Falls Church, VA 22042-5164

10. SPONSOR/MONITOR'S ACRONYM(S)

11. SPONSORING/MONITORING AGENCY REPORT NUMBER

12. DISTRIBUTION AVAILABILITY STATEMENT
Distribution A: Approved for public release

13. SUPPLEMENTARY NOTES

14. ABSTRACT

Due to their anisotropic shape, gold nanorods (GNRs) possess a number of advantages for biosystem use, including enhanced surface area and tunable optical properties within the near infrared region (NIR). However, a combination of cetyltrimethylammonium bromide (CTAB) related cytotoxicity, overall poor cellular uptake following surface chemistry modifications and loss of NIR optical properties due to material intracellular aggregation remain as obstacles for nano-based biomedical GNR applications. The current report demonstrated that in vitro exposure to tannic acid (TA) coated 11-mercaptoundecyl trimethylammonium bromide (MTAB) GNRs (MTAB-TA) in A549 human alveolar epithelial cells showed no significant decrease in cell viability or stress activation. In addition, MTAB-TA GNRs demonstrate a substantial level of cellular uptake while displaying a unique intracellular clustering pattern. This clustering pattern significantly reduces intracellular aggregation, preserving the GNRs NIR optical properties, vital for biomedical applications. MTAB-TA GNRs demonstrated significantly greater two photon luminescence microscopy image intensity and photo-thermal cellular ablation compared to bare MTAB GNRs. These results demonstrate how TA surface chemistry modification enhances biocompatibility and allows for a high rate of internalization while preserving the GNRs NIR optical properties. These findings identify MTAB-TA GNRs as prime candidates for use in nano-based bio-imaging and photo-thermal applications.

15. SUBJECT TERMS

16. SECURITY CLASSIFICATION OF: U			17. LIMITATION OF ABSTRACT	18. NUMBER OF PAGES	19a. NAME OF RESPONSIBLE PERSON
a. REPORT U	**b. ABSTRACT** U	**c. THIS PAGE** U			**19b. TELEPONE NUMBER (*Include area code*)** NA

Standard Form 298 (Rev. 8-98)
Prescribed by ANSI-Std Z39-18

i

THIS PAGE INTENTIONALLY LEFT BLANK.

TABLE OF CONTENTS

LIST OF FIGURES

LIST OF TABLES

PREFACE

THIS PAGE INTENTIONALLY LEFT BLANK.

1.0 SUMMARY

Due to their anisotropic shape, gold nanorods (GNRs) possess a number of advantages for biosystem use, including enhanced surface area and tunable optical properties within the near infrared region (NIR). However, a combination of cetyltrimethylammonium bromide (CTAB) related cytotoxicity, overall poor cellular uptake following surface chemistry modifications and loss of NIR optical properties due to material intracellular aggregation remain as obstacles for nano-based biomedical GNR applications. The current report demonstrated that *in vitro* exposure to tannic acid (TA) coated 11-mercaptoundecyl trimethylammonium bromide (MTAB) GNRs (MTAB-TA) in A549 human alveolar epithelial cells showed no significant decrease in cell viability or stress activation. In addition, MTAB-TA GNRs demonstrate a substantial level of cellular uptake while displaying a unique intracellular clustering pattern. This clustering pattern significantly reduces intracellular aggregation, preserving the GNRs NIR optical properties, vital for biomedical applications. MTAB-TA GNRs demonstrated significantly greater two photon luminescence microscopy image intensity and photo-thermal cellular ablation compared to bare MTAB GNRs. These results demonstrate how TA surface chemistry modification enhances biocompatibility and allows for a high rate of internalization while preserving the GNRs NIR optical properties. These findings identify MTAB-TA GNRs as prime candidates for use in nano-based bio-imaging and photo-thermal applications.

2.0 INTRODUCTION

Nanomaterials are increasingly being developed for use in industrial, military and consumer products, including a vast array of biomedical applications (Adlakha-Hutcheon et al., 2009; Barreto et al., 2011). Recent advances in solution chemistries for synthesis of solid phase nanomaterial technology make it possible to manipulate gold nanomaterials into different sizes, shapes and surface structures (Sun & Xia, 2002). Gold nanorods (GNRs) are of particular interest due to their unique optical region absorbance, emission and electronic properties. GNR optical properties are tunable by preparing nano-featured structure based upon their dimensional aspect ratio (AR) or through surface modification chemistry (Bouhelier et al., 2005). The AR describes the two dimensional proportional relationship between the nanomaterial's width and height. Depending on the GNR's AR, a narrow range of light frequencies induces conduction band electron oscillation, termed surface plasmon resonance (SPR) (Liang et al., 2012). The spectral signature of the GNRs longitudinal plasmon resonance extends into the near-infrared (NIR) region and GNRs with a longitudinal SPR between 650 and 950 nm fall within the non-absorbing region of water and carbon based substances, termed the "water window" (Weissleder, 2001). This feature allows for deep-tissue penetration and sensing with GNRs and makes them useful for nano-based biomedical applications. As such, GNRs have been used in a vast array of biomedical applications, including diagnostic imaging, photo-therapies, and drug/gene delivery (Agarwal et al., 2011; Nagesha et al., 2007; Pandey et al., 2013; Pissuwan et al., 2008). Further, GNRs also show great potential for "theragnostic" uses that combined diagnostic imaging and therapeutic applications (Choi et al., 2012; Jelveh & Chithrani, 2011; Wang et al., 2009; Yang et al., 2013). GNRs synthesized with AR 4 will have longitudinal SPR around 800nm, allowing for the interaction with readily available 800nm lasers and therefore making GNRs with an approximate AR of 4 an ideal theragnostic platform. However, the combination elicited toxicity, poor cellular uptake and loss of NIR optical properties due to intracellular aggregation remain as obstacles for using GNRs in many nano-based biomedical applications (Alkilany & Murphy, 2010; Panyala et al., 2009).

The toxicity of GNRs is largely a product of free and possibly surface associated cetyl trimethylammonium bromide (CTAB), which is a cationic surfactant used in the aqueous synthesis of GNRs (Takahashi et al., 2005; L. Wang et al., 2013a; Wang et al., 2011). During synthesis, CTAB provides a growth micelle environment around the gold seedings stabilizing them to form a rod (Jana et al., 2001; Nikoobakht & El-Sayed, 2003) and is present, in both the supernatant and as a bi-layer around the GNRs after synthesis. Two strategies have been reported to overcome this surfactant's cytotoxicity: 1) replacement by post-synthesis ligand exchange or non-covalent overcoating by chemical cover layering via electrostatic attraction (Vigderman et al., 2012a). Unfortunately, some commonly used surface modifications (e.g. polyethylene glycol; PEG) can significantly lower cellular uptake of the GNRs into cells, thus reducing their utility in biomedical applications (Grabinski et al., 2011; Huff et al., 2007). In addition, other surface modifications (e.g. polymer coatings, peptide functionalization etc.) are prone to particle aggregation when they are taken up by cells (Untener et al., 2013; Zhang et al., 2013c) and result in alteration and/or loss of key optical properties (Kelly et al., 2003; Sosa et al., 2003). Furthermore, over-coatings can break down in biological environments over time

(Ejima et al., 2013). This can result in surface leaching of the CTAB and therefore does not guarantee that the CTAB toxicity is completely mitigated by over-coating. Finally, over-coating and surface replacement procedures often require complicated multi-step functionalization processes (e.g. silica over-coating) that are difficult to scale up for biomedical applications (Gui & Cui, 2012).

Previous studies found that TA coated GNRs have reduced toxicity, demonstrate a distinctive form of endosomal uptake and display a unique intracellular distribution pattern that reduces particle aggregation (Debrosse et al., 2013; Untener et al., 2013). Unfortunately, as the CTAB-TA GNR's AR increases so does its toxicity, possibly due to any remaining CTAB. Therefore procedures for exhaustive removal or exchange of the CTAB from the GNRs may be essential to help lower toxicity. GNRs coated with MTAB (11-mercaptoundecyltrimethylammonium bromide), a thiol analogue of CTAB, represent a less toxic alternative though its biocompatibility and characterization within biological matrices has not yet been fully determined.

Vigderman et al. (2012b) recently used proton nuclear magnetic resonance spectroscopy to determine that complete replacement of CTAB with MTAB is possible due to its analogous chemical structure (Vigderman et al., 2012b). MTAB replacement occurs as CTAB micelle bilayer around the GNR is exchanged with a monolayer of MTAB that strongly binds to the GNR. This study found that MTAB GNRs had no toxicity in the human breast adenocarcinoma cell line, MCF-7 even at high concentrations (Vigderman et al., 2012b). In addition, 40% of MTAB GNR treatment was taken up by the cells, compared to less than 1% of their pegylated analogues, exceeding previously reported GNR uptake values (Vigderman et al., 2012b). However, Vigderman et al. (2012b) published TEM images that showed extensive aggregation of intracellular MTAB GNRs.This aggregation results in blue shift of plasmon resonance emissions, due to close proximity side by side assembly of GNRs, which moves the GNRs spectra MTAB GNRs out of the target NIR "water window" (Jain et al., 2006; Park, 2006). Therefore, new methods/techniques are needed to prevent the aggregation of MTAB GNRs in biological environment before they can be efficiently used in biomedical applications.

While the low toxicity and increased cellular uptake of MTAB GNRs are improvements over other GNR preparations, the loss of NIR optical properties described above limit their utility for biomedical applications.

2.1 Objective

The aim of this study is to address this limitation by combining MTAB replacement with TA over-coating (i.e. MTAB-TA GNRs) and comparing their properties relative to MTAB and Silica GNRs, as well as CTAB GNRs with and without TA over-coating. TA coated GNRs taken up by cells display a unique intracellular distribution pattern that appears to reduce particle aggregation (Alkilany et al., 2009; Untener et al., 2013). Due to this, it is hypothesized that MTAB-TA GNRs will exhibit enhanced biocompatibility and cellular uptake, while preventing particle aggregation to preserve key NIR optical properties within the A549 adenocarcinomic human alveolar basal epithelial cell line. The A549 cell line retains significant alveolar phenotype, and has been thoroughly characterized and used in numerous nano biocompatabilty, bio-imaging and therapeutic

studies (Foster et al., 1998; Kuo et al., 2012; Mason & Williams, 1980; Uboldi et al., 2009; Zhang et al., 2012b).

3.0 METHODS

3.1 Synthesis of gold nanorods
GNRs with an approximate AR 4 (MTAB, MTAB-TA, and Silica) were purchased from Nanopartz (Loveland, CO, USA). GNRs of approximately AR 3 (CTAB, CTAB-TA, PEG) were synthesized according to a modified seed mediated procedure reported by Park and Vaia (2008). Briefly, a seed solution of CTAB (0.1 M) and chlorauric acid (0.1 M) is combined at room temperature with a growth solution of CTAB (0.1 M), chlorauric acid (0.1 M) silver nitrate (0.1 M) ascorbic acid (0.1 M). The CTAB was purchased from GFS chemicals (Powell, OH, USA). The chloroauric acid, ascorbic acid, silver nitrate, sodium borohydride, sodium Chloride, MOPS buffer and tannic acid were obtained from Sigma Aldrich (St Louis, MO, USA).

3.2 PEG functionalization of GNRs
CTAB GNRs were functionalized with PEG as previously reported (Untener et al., 2013) with modifications. Briefly, the GNRs were functionalized overnight with 1 mM thiol PEG (Nanocs, Boston, MA) two times (MW 20000 followed by MW 5000) to displace the surface bound CTAB molecules. The GNR samples were centrifuged at 8,000g and the supernatant was removed and replaced with sterile water to remove residual free CTAB.

3.3 TA functionalization of GNRs
CTAB GNRs were functionalized with TA according to a modified procedure reported by Ejima et al. (2013) stepwise with TA (24mM), and MOPS buffer (100 mM, pH 7.4) with vortexing after each addition. The GNR samples were then centrifuged at 3,000g and the supernatant was removed and replaced with sterile water to remove residual TA. The MOPS buffer and tannic acid were obtained from Sigma Aldrich (St Louis, MO, USA).

3.4 Characterization of GNRs
The purity and spectral signature of the GNRs were analyzed before use with UV−Vis spectrometry on a Bio TEK Synergy HT (Winooski, VT, USA) instrument. For evaluation of rod size and morphology, nanoparticles in solution were placed onto a formvar carbon coated copper TEM grid (Electron Microscopy Sciences, Hatfield, PA, USA) and dried. They were imaged with transmission electron microscopy (TEM) using a Hitachi H-7600 with an accelerating voltage of 120 kV. To assess the surface charge of the GNRs, zeta potential measurements were taken using laser Doppler electrophoresis on a Malvern Zetasizer, Nano-ZS. Agglomerate sizes of the GNRs in media were determined through dynamic light scattering (DLS), also on a Malvern Zetasizer (Malvern Instruments, MA, USA).

3.5 Cell culture conditions

The A549 human lung cell line (American Type Culture Collection (ATCC), Manassas, VA, USA) was maintained in RPMI 1640 cell culture media (Life Technologies, Grand Island, NY, USA) supplemented with 10% fetal bovine serum (Hyclone, Logan, UT, USA) and 1% penicillin streptomycin. Cells were maintained in a humidified incubator controlled at 37 °C and 5% CO2. The same media composition was used for all GNR exposure procedures with the exception of the photo-thermal cellular ablation experiments where RPMI 1640 cell culture media without Phenol Red (Life Technologies, Grand Island, NY, USA) was used.

3.6 Cellular viability assessment
A549 human lung cell viability was evaluated using the CellTiter 96 Aqueous One Solution (MTS) (Promega, Madison, WI, USA) which monitors mitochondrial function and MultiTox-Glo Assay (LCDC) (Promega, Madison, WI, USA), which sequentially measures two protease activities; one is a marker of cell viability, and the other is a marker of cytotoxicity. Cells were seeded into a 96-well plate at a concentration of 2×10^3 cells per well and the following day treated with the stated GNR conditions. After exposure period, the cells viability was determined in accordance with the manufacturer's protocol. Result represents three independent trials with the average ± the standard error reported.

3.7 ROS assay
The intracellular generation of reactive oxygen species (ROS) after GNR exposure was evaluated using CM-H2DCFDA (Life Technologies, Grand Island, NY, USA) Technologies, Grand Island, NY) which is based on intracellular esterases and oxidation that yields a fluorescent product that is trapped inside the cell. Cells were seeded into a 96-well plate at a concentration of 2×10^3 cells per well and the following day treated with the stated GNR conditions. After 1 h, 6 h, and 24 h the intracellular ROS generation was determined in accordance with the manufacturer's protocol. Results represent three independent trials with the average ± the standard error reported.

3.8 RT-PCR for surfactant protein A and inflammatory gene expression
The A549 human lung cells were seeded in 6 well plates at a cell density of 6×10^5 cells/well cells/well. Following seeding and overnight incubation, the cells were treated with 20 µg/mL of GNRs, while untreated cells served as a negative control. Following 8 and 24 h of exposure, RNA was isolated using the RNeasy Mini Kit from Qiagen according to the manufacturer's protocols. The RNA quantity and purity was assessed using a NanoDrop 1000 and 1 µg of RNA was converted to cDNA using the High-Capacity cDNA Reverse Transcription Kit (Life Technologies, Grand Island, NY). The cDNA was then used in subsequent TaqMan® PCR assays to determine changes in gene expression for SPA1, Il-6, Il-6 and TNF -α and, while Hprt1 was used as a housekeeping gene to normalize expression changes. The gene expression was presented as a fold change determined using the 2ΔΔC(T) method (Livak & Schmittgen, 2001) and represents three independent trials with the average ± the standard error reported.

3.9 Human cytokine immunoassay

Secreted inflammatory proteins following GNR exposure were evaluated using the Bio-Plex Pro Human Cytokine 8-Plex Immunoassay (BIO-RAD, Hercules, CA). The multiplex assay detects the following cytokines: GM-CSF, IFN-γ, IL-2, IL-4, IL-6, IL-8, IL-10 and TNF-α. A549 cells were seeded in a 6-well plate at 6×10^5 cells/well for 24 h then exposed to GNRs (20 μg/mL) for 8 h. Next, the cells were washed three times with warm PBS, media was replaced and cells were incubated for 16 h. The media was then collected and cytokine concentration was determined in accordance with the manufacturer's protocol. Results represent three independent trials with the average ± the standard error reported.

3.10 Quantification of cellular uptake of GNRs by ICP-MS
A total of 1×10^5 cells/well were seeded on 12mm diameter glass slides in a 24-well plate in triplicate then dosed with 5 μg/mL GNRs for 24 h. The cell samples were then washed three times with warm PBS and digested with an aqueous solution containing 0.05% Triton X-100, 3% HCl, and 1% HNO_3. For GNR retention study the cell samples were then washed three times after 24 h post-exposure with warm PBS and media was replaced and repeated on day 4 and day 8. The intracellular gold concentration was determined through inductively coupled plasma mass spectrometry (ICP-MS) on a Perkin-Elmer ICP-MS 300D instrument (Santa Clara, CA). ICP-MS was conducted in standard mode with 20 sweeps per reading, at one reading per replicate, and three replicates per sample with a dwell time of 100 ms. A calibration curve was obtained using four gold standard solutions and the addition of an internal standard was done to ensure that no interferences were occurring. Results represent three independent trials with the average ± the standard error reported.

3.11 Darkfield microscopy
A549 human lung cells were seeded at 1.25×10^5 cells per chamber on a 2-well chambered slide and grown for 24 h. The following day the cells were dosed with 20 μg/mL GNRs for 24 h. After 24 h, the cells were fixed with 4% paraformaldehyde and incubated with Alexa Fluor 555-phalloidin for actin staining and DAPI for nuclear staining (Life Technologies, Grand Island, NY). The slides were then sealed and imaged using a CytoViva 150 ultra resolution attachment on an Olympus BX41 microscope (Aetos Technologies, Opelika, AL). All experiments were performed at a minimum of three times. Care was taken to ensure full evaluation of each slide for well represented images**.**

3.12 Transmission electron microscopy
A549 human lung cells were seeded in a 6-well plate at 6×10^5 cells/well for 24 h then exposed to the stated GNRs concentration (5 and 20 μg/mL) and washed three times with warm PBS. The cells then fixed overnight in 2% paraformaldehyde and 2% glutaraldehyde after indicated duration (24 h, 4 days or 8 days). The cells were then stained with 1% osmium tetroxide, washed, and subsequently dehydrated with ethanol dilutions ranging from 50 to 100%. The cells were then embedded in LR White resin and cured overnight at 60 °C under a vacuum, after which the samples were sectioned using a Leica EM UC7 Ultramicrotome. Cell sections of 70 nm in thickness were placed on a Formvar carbon coated copper TEM grid (Electron Microscopy Sciences, Hatfield, PA)

and were imaged. Transmission electron microscopy (TEM) was performed using a Hitachi H-7600 with an accelerating voltage of 120kV. All experiments were performed at minimum three times. Care was taken to ensure full evaluation of each sectioned sample for well represented images.

3.13 Hyperspectral microscopy

A549 human lung cells were seeded at 1.25×10^5 cells per chamber on a 2-well chambered slide and grown for 24 h and the following day was exposed to GNR (20ug/ml). After 24 h, the cells were fixed with 4% paraformaldehyde. The slides were then sealed and imaged using a CytoViva Hyperspectral Imaging System (Auburn, AL). Image capture times and setting remained constant for all samples. Finally, hyperspectral analysis was performed using CytoViva's hyperspectral image analysis software. Results represent three independent trials with the average ± the standard error reported. Care was taken to ensure full evaluation of each slide for well represented images.

3.14 Two-photon luminescence microscopy

A549 cells were seeded at 1.25×10^5 cells per chamber on a 2-well chambered slide and grown for 24 h and the following day was exposed to GNR (20μg/ml). After 24 h, the cells were fixed with 4% paraformaldehyde. The slides were then sealed and imaged using an Olympus fv100 multi-photon confocal microscopy Imaging System with a 25x (NA 1.05) water immersion objective (Center Valley, PA). Ti-sapphire laser (Mia-Tai laser, Spectra-Physics, Mountain View, CA) at 810 nm set at 0.5% transmissivity was used as excitation light source and a two-photon luminescence emission was detected by a photomultiplier tube with an ET660/40m-2p (640-680 nm) band pass filter (Chroma Technology, Bellows Falls, VT, USA). Cells were imaged at four times zoom and 0.15 μm/slices though the cells were captured. Image capture setting remained constant for all samples. Finally, image processing and intensity analysis was performed using Olympus's Fluoview (Center Valley, PA) image analysis software. Extracellular MTAB GNRs were used as an image intensity control. Results represent two independent trials (minimum of 8 replicates per trial) with the average ± the standard error reported.

3.15 Plasmonic photo-thermal cells ablation

A549 cells were seeded in a 6-well plate at 6×10^5 cells/well for 24 h then exposed to GNRs (20 μg/mL) and washed three times with warm PBS. Cells were then exposed to the cell-permeant calcein AM (2 μM) (Life Technologies, Grand Island, NY) and the non-cell-permeant ethidium homodimer-1 (4 μM) (Life Technologies, Grand Island, NY) and after 15 min cells were irradiated with an 810nm 3W Ti-sapphire laser (Mia-Tai laser, Spectra-Physics, Mountain View, CA) for 60 sweeps at indicated power level. Cellular ablation was measured at the 0, 1, 5, 10 min time points. Results represent four independent trial with the average reported. Care was taken to ensure full evaluation of each slide for well represented images.

3.16 Statistical analysis

All experimental results represent a minimum of three independent trials unless otherwise stated. Data were expressed as the mean ± the standard error of the mean (SEM).

Statistical calculations were performed using SAS (Version 9.1) or GraphPad Prism (version 5.02, GraphPad Software Inc. La Jolla, CA, USA) to determine statistical significance at p values of <0.05 (*), <0.01 (**) , or <0.001 (***).

4.0 RESULTS AND DISCUSSION

4.1 GNR characterization

GNR characterization was performed to determine their key physicochemical properties and to verify particle uniformity prior to experiments. TEM images demonstrated that GNR sets were uniform in size and morphology (Figure 1 and Table 1). The AR 4 GNRs had a diameter 24.5 ± 1.1 nm and a length of 104 ± 1.2 nm on average. UV−Vis analysis confirmed predicted SPR peaks based on calculated AR (Figure 1D & H) (Jun et al., 2008). To determine GNR surface charge, zeta potential analysis was performed on each particle (Table 1). From this analysis, it was shown that MTAB GNRs were positively charged as expected due to MTABs quaternary ammonium cation. MTAB-TA GNRs displayed a negative surface charge, indicating that functionalization with TA was successful. When the GNRs were exposed to a protein rich environment (culture media) both MTAB and MTAB-TA GNRs displayed a negative surface charge, -15.5 and -18.1 mV respectively. Hydrodynamic size of GNRs in culture media showed that TA coated GNRs were on average larger than MTAB GNRs.
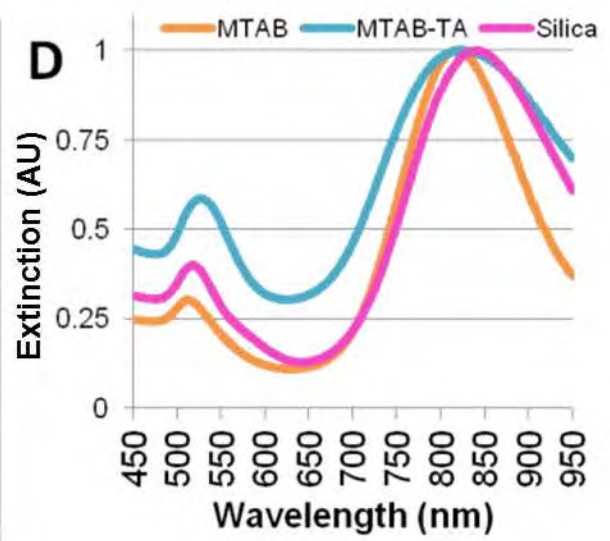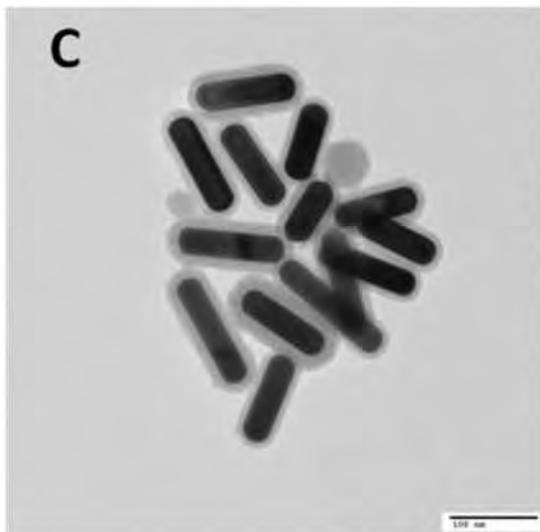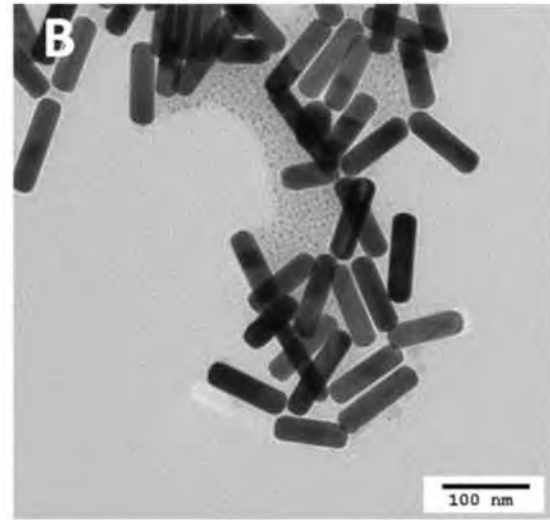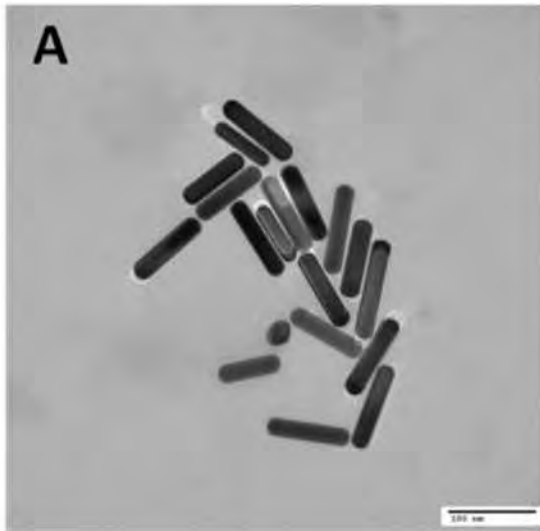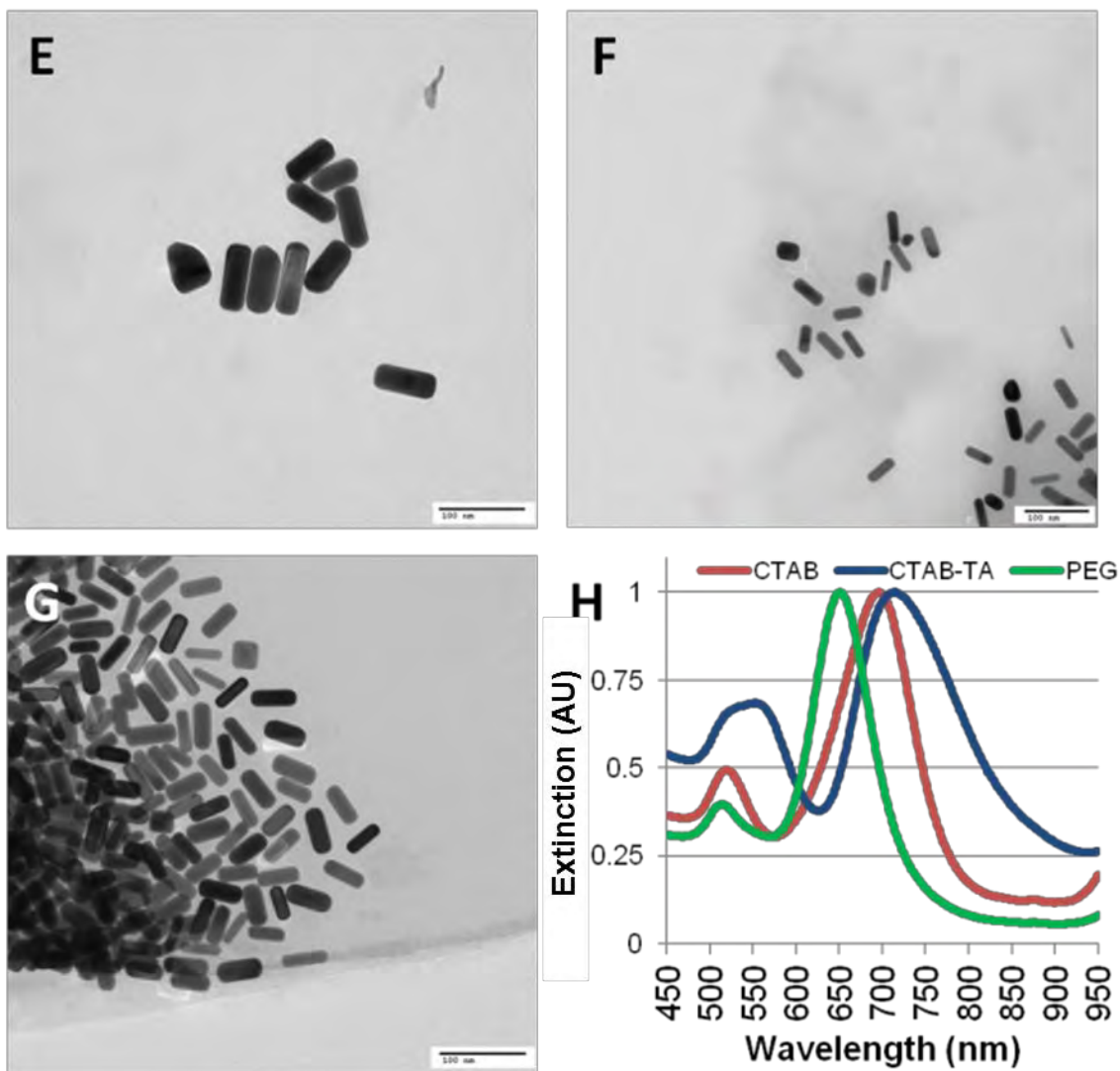
Figure 1. GNR characterization.
Representative TEM images of A. MTAB, B. MTAB-TA and C. Silica; D. UV-Vis absorption spectra of MTAB (gold), MTAB-TA (light blue) and Silica (pink) GNRs. Representative TEM images of E. CTAB F. CTAB-TA and G. PEG. H. UV-Vis absorption spectra of CTAB (red), CTAB-TA (dark blue) and PEG (green) GNRs.

Table 1. **Characterization of GNRs**

Name	Primary Size (nm)	Aspect Raito	Surface Chemistry	Surface Charge (mV)	Hydrodynamic Diameter in Media (nm)
MTAB	25x102 ±4.0	4.1	MTAB	36.0	288.2 ±9.5
MTAB-TA	25x104 ±2.8	4.1	MTAB-TA	-15.7	509.6 ±66.9
Silica	25x106 ±3.0	4.2	Mesoporous Silica	11.6	455.8 ±11.3

10

CTAB	25x72 ±3.1	2.9	CTAB	37.2	318.7 ±4.3
CTAB-TA	22x60 ±2.1	2.8	CTAB-TA	-19.4	416.4 ±35.2
PEG	19x48 ±2.6	2.5	PEG	2.1	75.2 ±0.9

4.2 MTAB-TA GNRs display enhanced biocompatibility

Since GNRs are known to exhibit toxicity linked to their physiochemical properties, we compared the biocompatibility of CTAB and MTAB GNRs with and without TA coating by evaluating membrane integrity and mitochondrial function (Figure 2). Overcoating CTAB and MTAB GNRs with TA resulted in enhanced biocompatibility, with no significant decrease in viability with exposure to MTAB-TA GNRs concentrations as high as 320 µg/mL (Figure 2B). Following exposure to MTAB and MTAB-TA GNRs (20 µg/ml), A549 cells showed no significant effects on their cellular viability with viability remaining over 95% after 24 h and 48 h (Figure 2 A & C). The viability data demonstrated that the reported toxicity of CTAB-TA was not due to the TA over-coating, negative surface charge or the AR of these GNRs, suggesting that the residual CTAB bilayer was the cause of the toxicity (Alkilany et al., 2009).

Next, cellular stress was examined by measuring changes in reactive oxygen species (ROS) after cellular exposure to the GNRs. The 6 h time point was chosen based on maximum ROS response before cell death. A549 cells showed no significant increase in ROS levels after exposure to MTAB and MTAB-TA GNRs, even at four times the treatment concentration of the CTAB GNRs that significantly increased ROS levels (Figure 2D).

Finally, GNR surface chemistry has been shown to alter cellular response, and gene and protein expression analysis has been used to detect subtle changes after exposure to GNRs and other NMs (Grabinski et al., 2011; Hauck, et al., 2008b). Therefore, we evaluated the inflammatory response of exposure to MTAB and MTAB-TA GNRs in A549 human lung cells by measuring changes in surfactant protein A (SPA1) and inflammatory cytokine (SPA1, IL-6, IL-8 and TNF-α) mRNA expression and GM-CSF, IFN-γ, IL-2, IL-4, IL-6, IL-8, IL-10 and TNF-α cytokine release.

A549 cells showed no significant change in the measured mRNA (SPA1, IL-6, IL-8 and TNF -α) levels after 8 h and 24 h (Figure 3) exposure to MTAB and MTAB-TA GNRs (20µg/mL). However, a lower concentration of CTAB GNRs (2.5µg/mL) resulted in a significant increase of IL-6, IL-8 and Tnf-α mRNA after 8 h and SPA1, IL-8 and Tnf-α mRNA after 24 h.

In addition there was no significant change in GM-CSF, IFN-γ, IL-2, IL-4, IL-6, IL-8, IL-10 and TNF-α cytokine release after exposure to MTAB and MTAB-TA GNRs (20µg/mL). Overall cytokine release was low with only GM-CSF and IL-8 cytokines reaching concentrations greater than 1pg/mL (Figure 4). Together these results demonstrated the high *in vitro* biocompatibility of both MTAB and MTAB-TA GNRs. In view of their biocompatibility based on these initial findings and their longitudinal SPR peaks in the NIR "water window", we chose to further explore the cellular association and *in vitro* hyperspectral signature of MTAB GNRs with and without a TA coating.
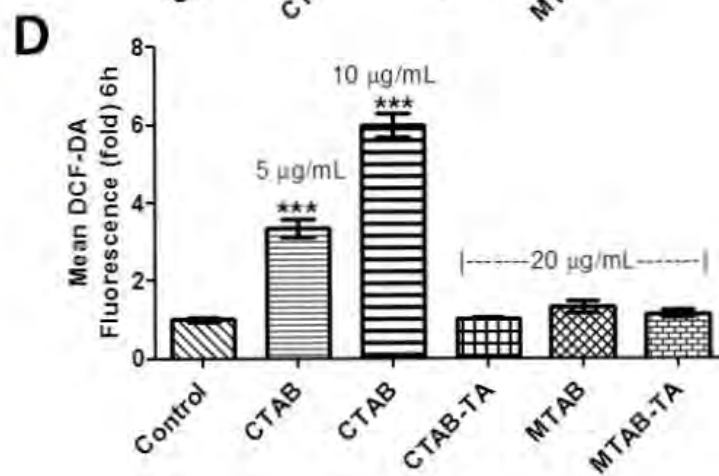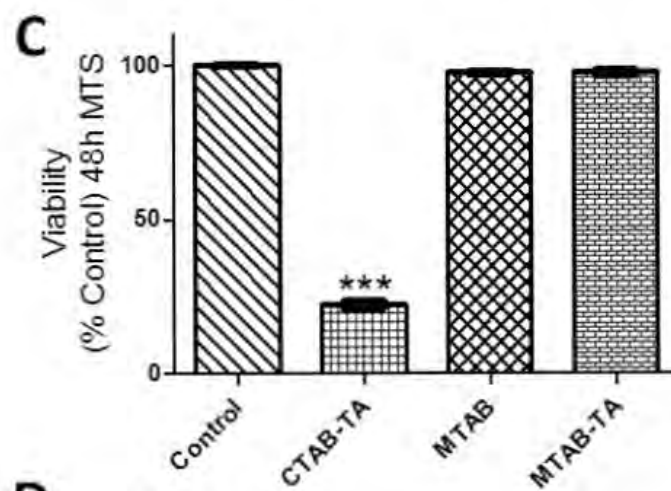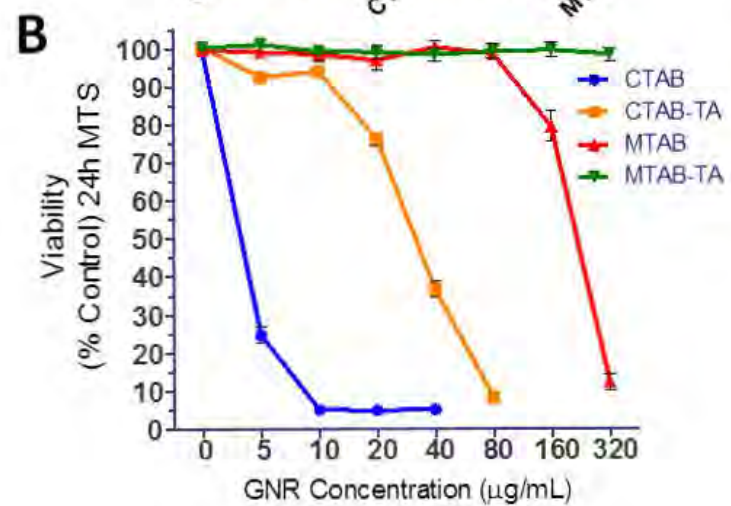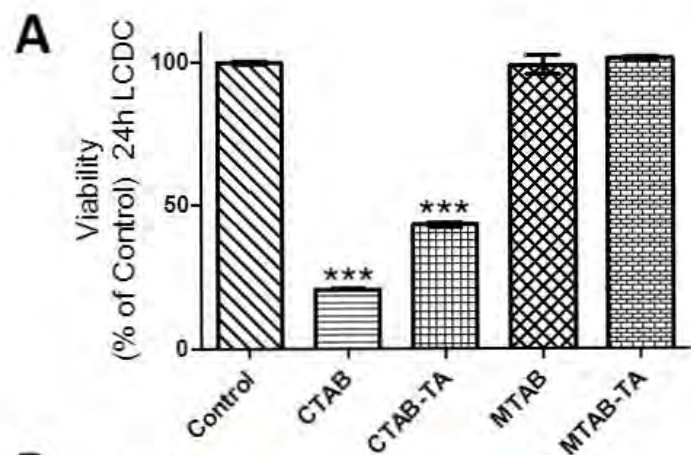
Figure 2. MTAB-TA GNRs demonstrate enhanced biocompatibility.
A549 human lung cells were exposed to MTAB and MTAB-TA GNRs for 24 h or 48 h.
Cell viability was assessed using LCDC or MTS assays and was represented relative to
the control cells. A. LCDC assay showed no significant decrease in cell viability
following exposure (20 µg/mL) for 24 h.. However, exposure to CTAB and CTAB-TA
GNRs (20 µg/mL) resulted in a significant decrease in cell viability. B. 24 h MTS assay
results indicated that the TA coating enhanced the biocompatibility of both CTAB and
MTAB GNRs. MTAB –TA showed no significant decrease in viability at concentrations
as high as 320 µg/mL C. 48 h MTS assay showed that the cytotoxicity of CTAB-TA
GNRs (20 µg/mL) significantly increases over time whereas there was no significant
decrease in viability after exposure to MTAB and MTAB-TA GNRs. D. ROS assay
demonstrated no significant increase in ROS after exposure to CTAB-TA, MTAB and
MTAB-TA GNRs. Taken together, these results demonstrate the high biocompatibility of
both MTAB and MTAB-TA GNRs. Statistical significance was determined using a one
way ANOVA with Dunnett's post-hoc tests.
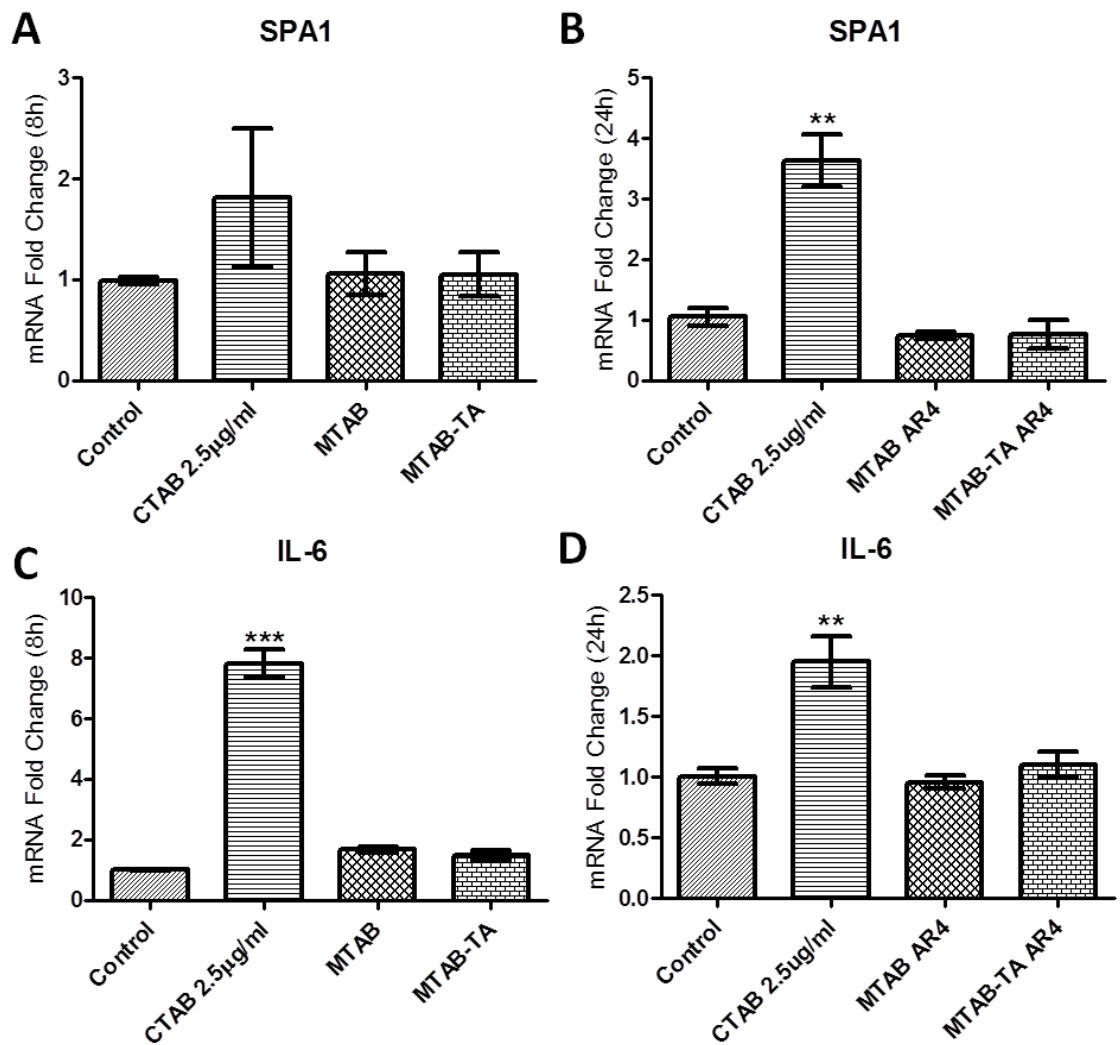
Figure 3. MTAB-TA GNRs do not alter inflammatory gene expression.
A549 human lung cells were exposed to GNRs for 8 h and inflammatory gene expression was assessed at 8 h and 24 h using RT-PCR. MTAB and MTAB-TA GNRs (20μg/mL) resulted in no significant change in A-B. SPA1, C-D. IL-6, E-F. IL-8 and G-H. TNF -α mRNA levels after 8 h or 24 h. In contrast, CTAB GNRs (2.5μg/mL) resulted in a significant increase of IL-6, IL-8 and TNF -α mRNA after 8 h and SPA1, IL-8 and TNF -α mRNA after 24 h in A549 human lung cells. Statistical significance was determined using a one-way ANOVA with a tukey post-hoc tests.
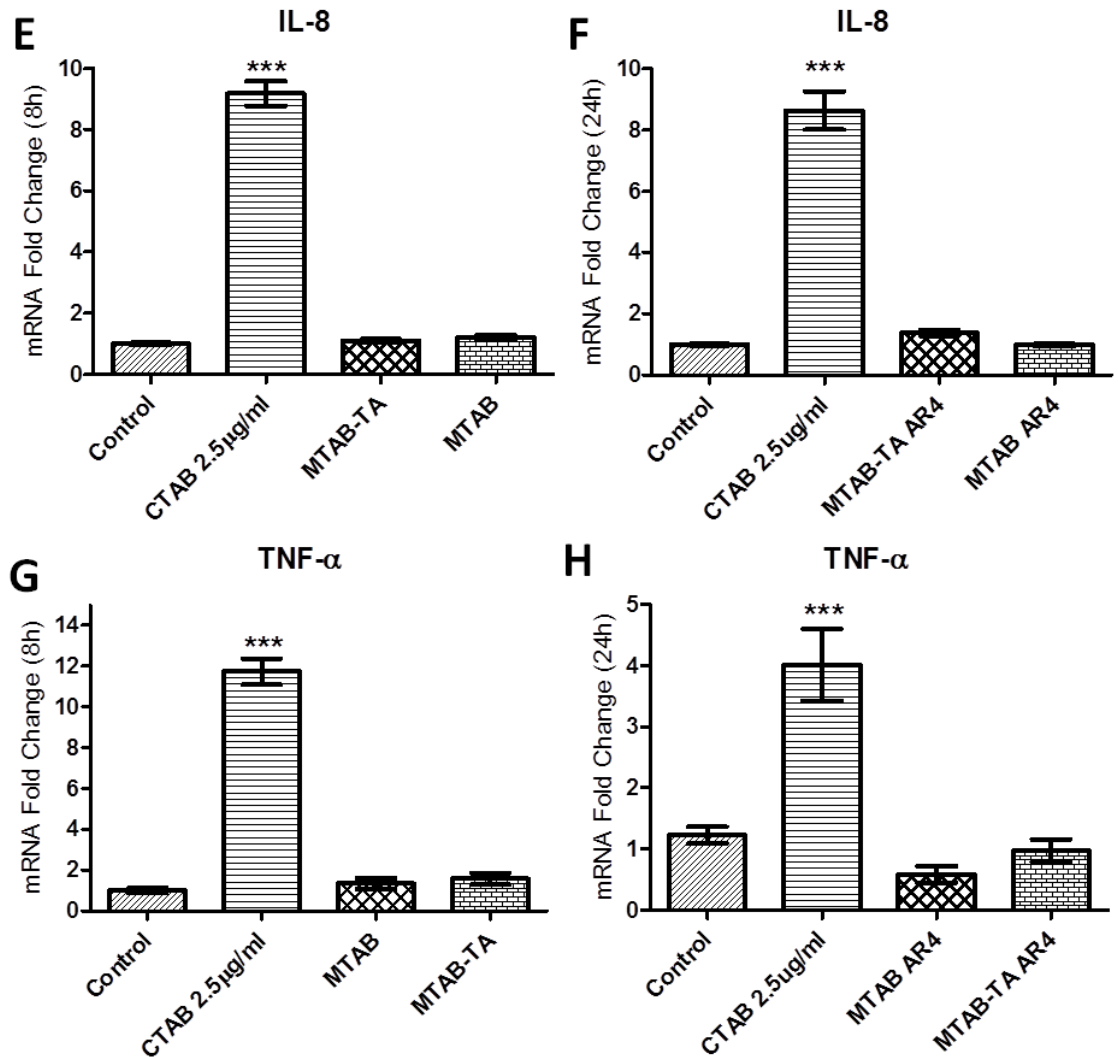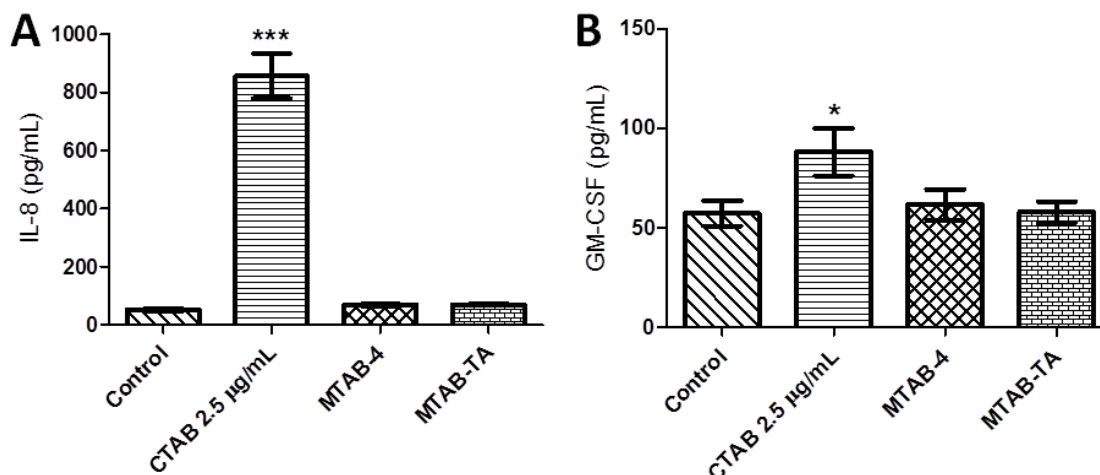
**Figure 4. MTAB-TA GNRs do not alter cytokine release.**
A549 human lung cells were exposed to GNRs for 8 h and inflammatory gene expression was assessed at 24 h using a multiplex bead-based flow cytometric immunoassay. MTAB and MTAB-TA GNR exposures (20µg/mL) resulted in no significant change in released A) IL-8 and B) GM-CSF protein levels. Exposure to CTAB GNRs (2.5µg/mL) resulted in a significant increase of released IL-8 and GM-CSF protein in A549 human lung cells. Statistical significance was determined using a one-way ANOVA with a tukey post-hoc tests.

4.3 Cellular association and *in vitro* intracellular hyperspectral signature of MTAB-TA GNRs

Visualization of cellular association of MTAB and MTAB-TA GNRs was examined using darkfield microscopy (Figure 5A-C). Both GNRs interacted with A549 cells and had a high level of cellular association. MTAB and MTAB-TA GNRs appeared to be densely packed, suggesting the associated and/or internalized GNRs are in clusters. In addition the morphology of A549 cells were retained, further confirming the biocompatibility of the GNRs.

Next, we performed *in vitro* hyperspectral imaging (HSI) microscopy to investigate the GNR optical properties after cellular association. HSI combines the use of darkfield microscopy and spectroscopy for the measurement of the reflectance spectrum at individual pixels in a micrograph. HSI analysis has successfully been used for characterizing gold nanoparticle aggregation, protein adsorption and cell uptake in biological/cellular environments (Grabinski et al., 2013). This *in vitro* analysis of MTAB and MTAB-TA GNRs is critical, as many studies have shown that biological/cellular environments can alter the optical properties of GNRs and other nanomaterials. HSI analysis demonstrated that both GNRs had a strong association to A549 cells and appeared to indicate clustering of both MTAB and MTAB-TA GNRs (Figure 5D-E). However, the MTAB GNRs displayed a vast array of colors when compared to the primarily white appearance of the MTAB GNRs, indicating a shift out of the NIR to the visible spectra. Further, MTAB-TA GNRs have a more uniform clustering that allows for easier identification and delineation of the GNR clusters. Next, the reflectance spectrum of individual GNR clusters were measured and compiled to create a hyperspectral profile

for both MTAB and MTAB-TA GNRs (Figure 5G). The hyperspectral analysis revealed that the spectral maximas were decreased in both hyperspectral profiles, as compared to their spectral profiles as synthesized (Figure 13). This blue shift in spectral maximas could have resulted from GNR intracellular aggregation with side-by-side assembly (Jain et al., 2006; Stacy et al., 2013). This would effectively lower the GNR AR resulting in the changes seen in hyperspectral profile. The hyperspectral profile of MTAB-TA GNRs (n=385) revealed a sharper peak still within the NIR target "water window" (~732 nm). In contrast, the hyperspectral profiles of MTAB GNRs (n=194) and control (n=335) displayed broad peaks that were located primarily outside the target NIR window (~630-679 nm and ~550-634 nm, respectively). In addition, MTAB-TA GNRs demonstrated a greater than 2.5 fold increase in scattering intensity after cellular association over the MTAB GNRs. Together, these results suggest that the MTAB-TA GNR form uniform GNR clusters that are able to preserve their NIR optical properties after cellular uptake. This finding is significant for nano-based bio-imaging and therapeutic applications as a strong spectral profile in the NIR "water window" after exposure to biological/cellular environments is required for optimum efficacy in biomedical applications.

One possible explanation of the differences in hyperspectral signature may be due to differences in GNR uptake. Another possible explanation could be due to differences in aggregation states after cellular association and/or internalization (Aaron et al., 2009). To test these possibilities, we set out to examine MTAB and MTAB-TA GNR uptake by Inductively Coupled Plasma Mass Spectrometry (ICP-MS) and intracellular aggregation states by TEM.
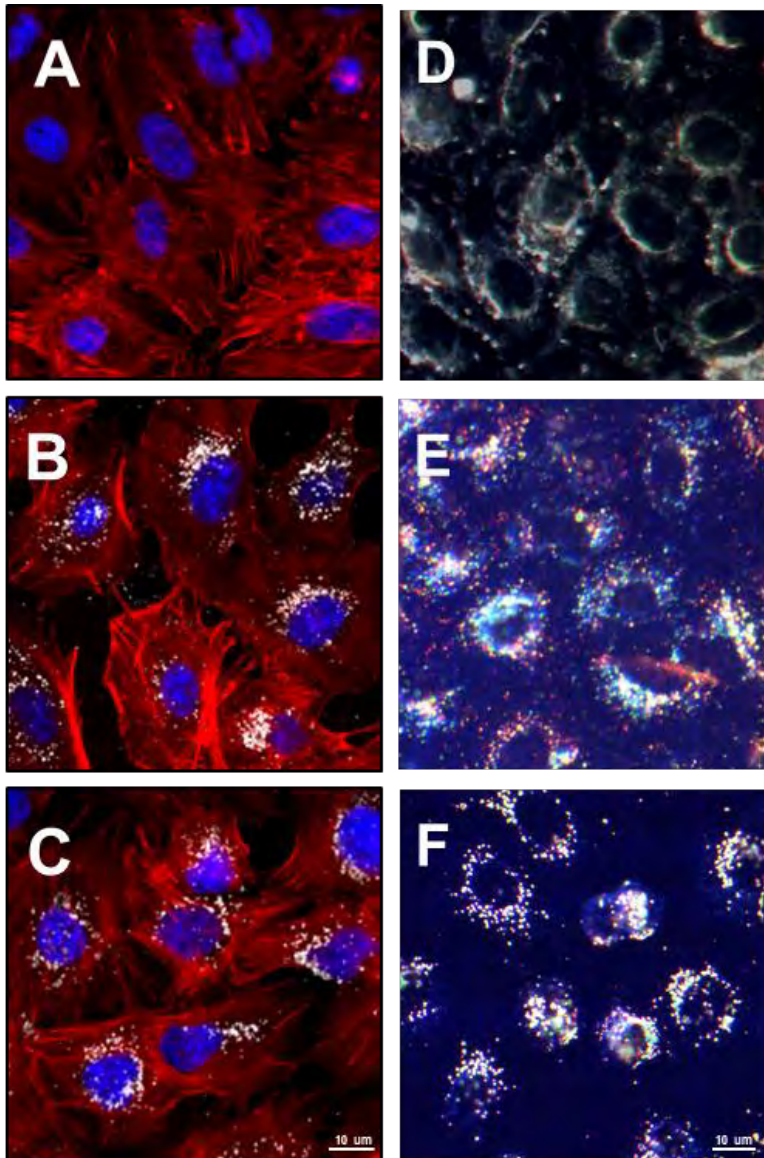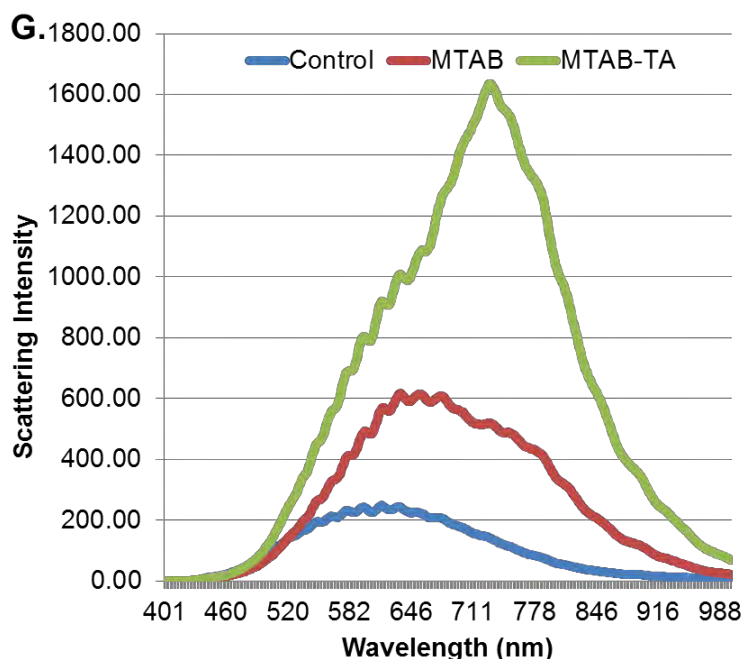
Figure 5. Intracellular MTAB-TA GNRs retain NIR optical properties.
Representative darkfield and hyperspectral images of A549 cells with analysis of intracellular GNR optical properties. Fluorescent images following 24 h exposure to GNR (20 µg/mL) A. Control, B. MTAB and C. MTAB-TA. Fluorescent images illustrate clustering of GNRs with the morphology of A549 cells retained. A549 cells underwent actin (red) and nuclear (blue) staining with GNRs (reflecting white). Hyperspectral images following 24 h exposure to GNR (20 µg/mL) D. Control, E. MTAB and F. MTAB-TA. Results revealed that MTAB-TA presented a more uniform clustering and spectral profile based on their appearance in the hyperspectral images. G. Analysis of *in vivo* optical properties. MTAB hyperspectral profile (red) (n=194) displayed low intensity and loss of NIR optical properties of GNRs. In contrast, the MTAB-TA hyperspectral profile (green) (n=385) showed preserved NIR properties with intensity greater than 2.5 times that of the MTAB hyperspectral profile. Control (blue) (n=335).

4.4 High uptake with unique clustering pattern of MTAB-TA GNRs
Quantification of cellular uptake in the MTAB and MTAB-TA GNRs (5 µg/ml) was determined by ICP-MS. Both MTAB and MTAB-TA GNRs showed a high level (40% and 39% of treatment respectively) of cellular uptake compared to 1.5% with PEG GNRs or 15% with silica coated GNRs (Figure 6A). These results are similar to the 40% uptake of MTAB GNRs in MCF-7 cells reported by Vigderman et al (Vigderman et al., 2012b). In addition, this finding suggests that the TA over-coating negative surface charge has minimal impact on cellular uptake of MTAB-TA GNRs. These findings appear to differ from other studies that report that GNRs with a positive surface charge have a greater cellular association and uptake than GNRs with a negative surface charge (Hauck et al., 2008a; Qiu et al., 2010). It was originally proposed that the positive surface charge on the GNRs was attracted to the negatively charged membrane of the cell resulting in higher GNR cellular association (Hauck et al., 2008a). However, when GNRs of

differing charge are placed in a biological environment (or simulated biological environment such as culture media) the GNRs will take on the charge of the biological environment (Qiu et al., 2010). This is in agreement with our finding that both MTAB and MTAB-TA GNRs displayed a negative surface charge, -15.5 and -18.1 mV, respectively. It has been more recently proposed that the greater uptake levels seen with GNRs with a positive surface charge is because of their greater affinity for protein and formation of a protein corona that strongly influences the GNRs cellular uptake (Nel et al., 2009; Qiu et al., 2010; Walkey & Chan, 2012; Walkey et al., 2014). TA has a strong attraction for protein and cellular membranes that has been well documented (Van Buren & Robinson, 1969; Wagner, 1976). In addition, it has been reported that TA coated gold NMs have strong cellular association and unique form of cellular uptake (Mukhopadhyay et al., 2012; Untener et al., 2013). Therefore the MTAB-TA GNRs may form a distinctive protein corona that may account for their uptake properties; thus, further research on the impact of the protein corona of TA GNRs and other NM is needed. The finding that there is no significant difference in uptake of the two GNRs further suggests that the difference seen in hyperspectral profiles is not significantly impacted by differences in cellular uptake of the two GNRs.

The concentration of GNR remained at that level for up to 8 days post exposure with 93% and 90% retention of the MTAB and MTAB-TA GNRs, respectively (Figure 6B). This suggests that there is minimal exocytosis of the GNRs and/or high reuptake of exocytosed GNRs as supported by the previous finding on GNR trafficking (Zhang, W. et al., 2013a). Therefore, we investigated the intracellular state of the GNRs, as previous studies have shown that the aggregation state of GNRs can affect their spectral profiles (Kelly et al., 2003; Sosa et al., 2003).

The distribution of MTAB and MTAB-TA GNRs (5 µg/ml) within the cell was observed using TEM (Figure 7). MTAB-TA GNRs demonstrated low aggregation of GNRs with a unique distribution pattern/clusters within the A549 cells. In contrast, MTAB GNRs appeared aggregated in dense clusters and/or tightly packed crest shape groupings. This suggests aggregation of the MTAB GNRs in the cell may account for the differences seen in the two GNRs spectral profiles after cellular association.
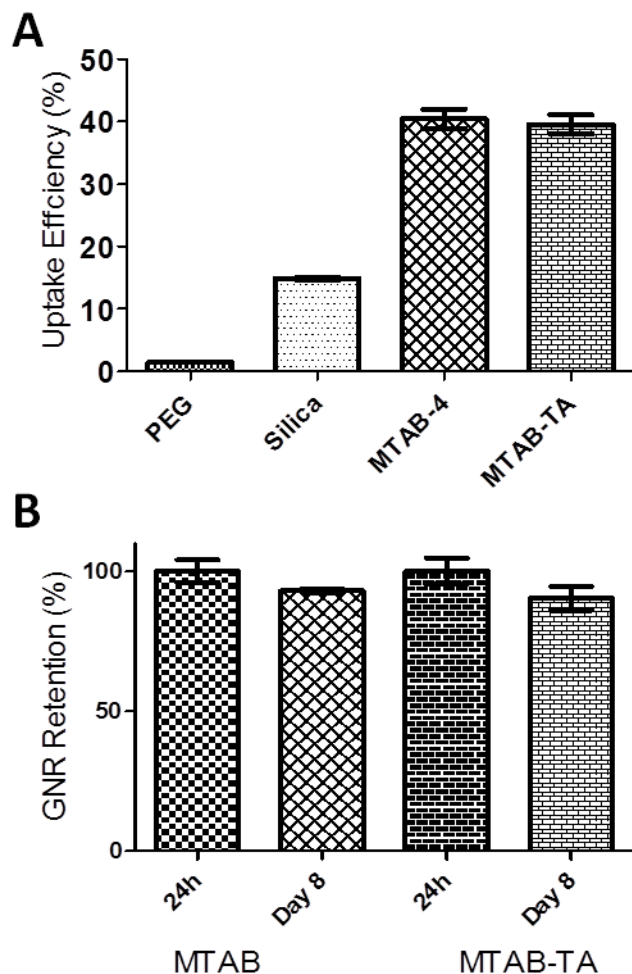
Figure 6. Uptake and retention of MTAB-TA GNRs
A549 human lung cells were exposed to GNRs (5 μg/mL) for 24 h, GNR uptake was quantified using ICP-MS. A. Results show high level of uptake of 40% for MTAB and 39% for MTAB-TA GNRs compared to PEG (1.5%) and Silica (15%) GNRs. B. After 8 days post exposure 93% and 90% of the MTAB and MTAB-TA GNRs were retained, respectively. Statistical significance was determined using a one-way ANOVA with a Tukey post-hoc tests.

Figure 7. Visualization of MTAB-TA GNR uptake.
Representative TEM Images of A549 cells after 24 h GNR exposure (5µg/ml). A. MTAB
B. MTAB-TA C. Control. Results demonstrated intracellular aggregation of MTAB
GNRs and low aggregation of MTAB-TA GNRs.

4.5 Low intracellular aggregation of MTAB-TA GNRs.
Since concentration can influence nanoparticle aggregation, we studied this cellular
patterning at 20 µg/ml. At this new concentration, MTAB GNRs displayed small and
large tightly packed clusters (Figure 8 A1,A4), crest (Figure 8 A3,5,6) and doughnut
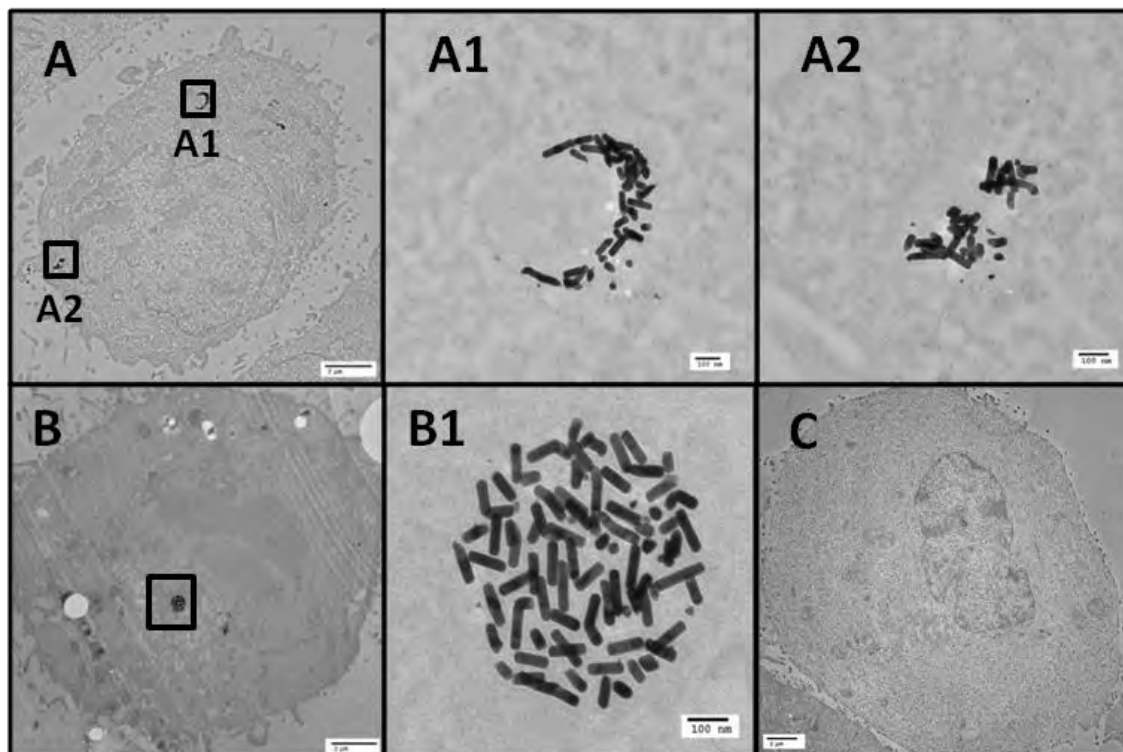(Figure 8 A2) shaped groupings with aggregation of GNRs. MTAB-TA GNRs again
displayed distinctive GNR cluster patterns with low aggregation of GNRs (Figure 8 B).
Most GNRs are taken up through receptor-mediated endocytosis and further trafficked
via an endo-lysosomal pathway (Chithrani et al., 2009). Further, it appears that the
MTAB-TA GNR clusters are less compressed/density packed than the MTAB GNR
groupings. After 8 day post exposure the number of GNR clusters/groupings per cell in
both the MTAB and MTAB-TA exposed cells decreased possibly due to consolidation of
the GNR groupings and by cell division (Figure 9). However, there is only a slight
decrease in the total amount of GNRs present in the sample (Figure 6B). This supports
the finding of Zhang et al (2013a) that demonstrated the long term retention of gold
nanoparticles in NDA-MB-231 breast cancer cells with the concentration of GNRs in
cells correlating with their rate of cellular division rather than exocytosis.
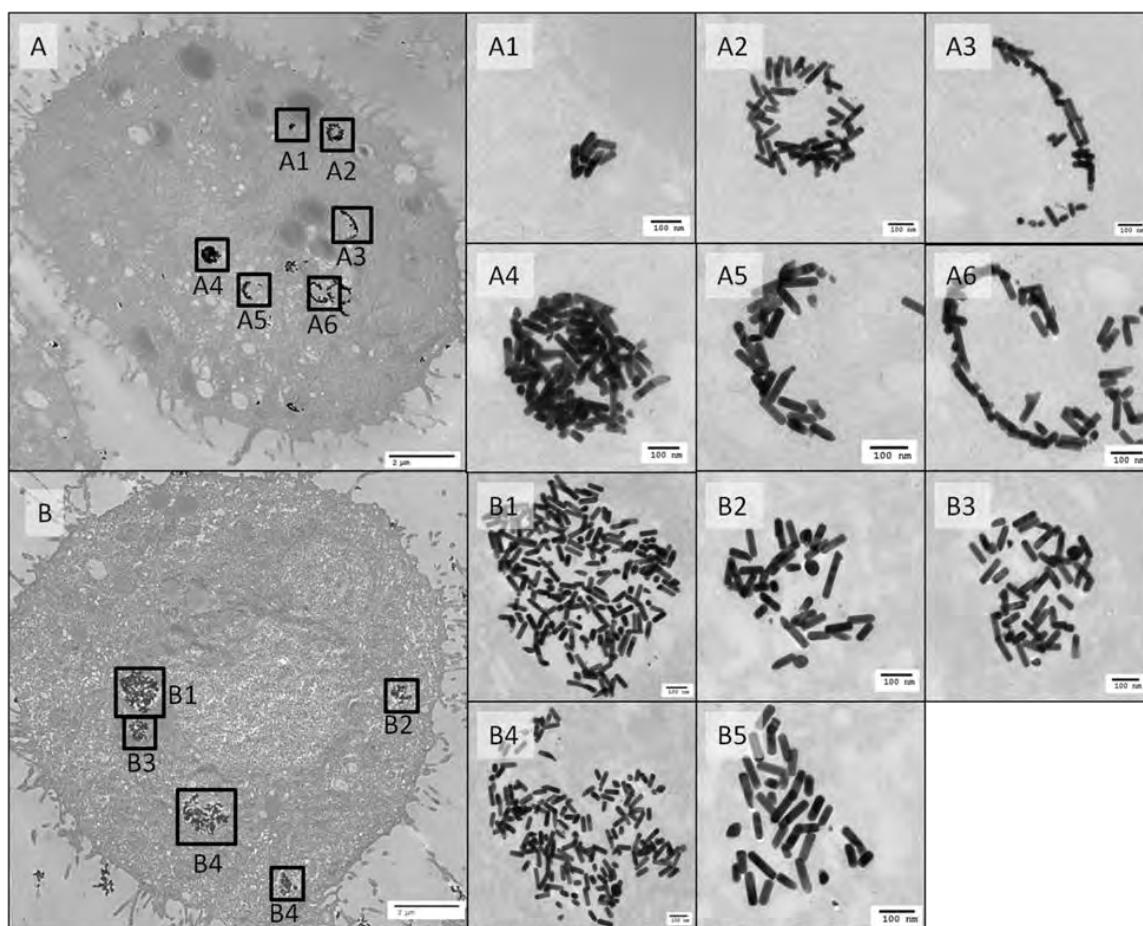
Figure 8. Visualization of intracellular clustering pattern of MTAB-TA GNRs. Representative TEM Images of A549 cells after 24 h GNR exposure (20μg/ml). A. MTAB and B. MTAB-TA GNRs. Results demonstrate intracellular aggregation of MTAB GNRs and low aggregation and unique clustering of MTAB GNRs.
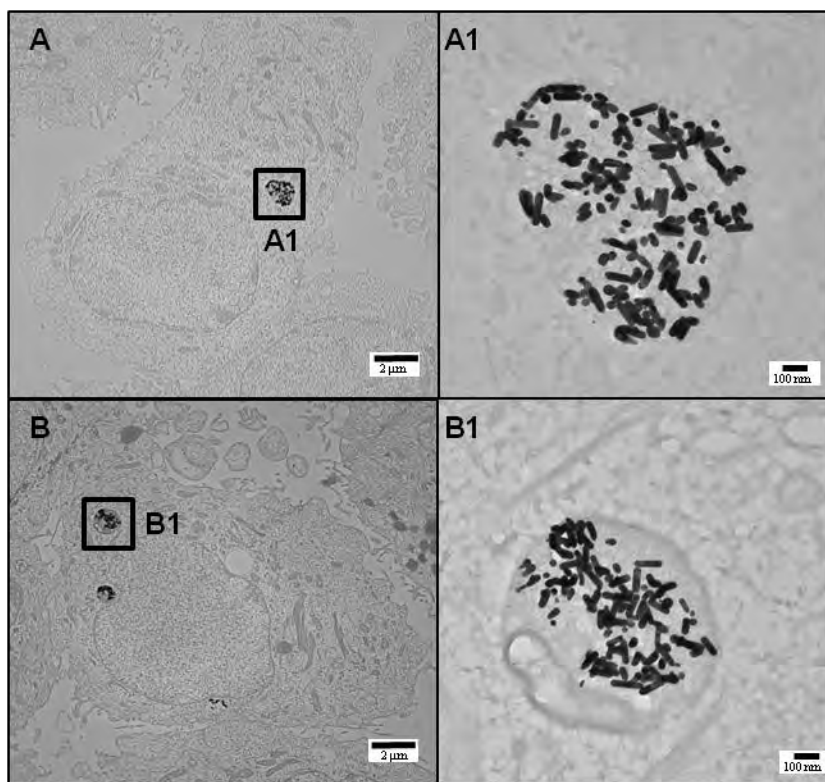
Figure 9. Visualization of MTAB-TA GNRs cellular retention.
Representative TEM Images of A549 cells 8 day post exposure after 24 h GNR exposure
(20μg/ml). Representative images of A. MTAB and B. MTAB-TA GNRs 8 days post
exposure. Results show a decrease in the number of GNR clusters/groupings per cell in
both the MTAB and MTAB-TA exposed cells.

Next, we analyzed the GNRs clusters/groupings with ImageJ software (Schneider
et al., 2012) (Figure 10). The MTAB GNR groupings (n=28) were more densely packed
than the MTAB-TA GNR groupings (n=24) as reflected in the area fraction of GNRs
over total area of clusters/groupings values of 64% vs 50%, respectively (p<0.001). In
addition, the MTAB GNR groupings had a smaller average diameter (calculated as the
mean of smallest and largest diameter measurement for each grouping) than the average
MTAB-TA GNR cluster at 343 nm vs 534 nm, respectively (p<0.001). The total area of
the MTAB-TA GNR clusters, as measured by ImageJ, appears to trend larger; however,
the difference was determined not to be statistically significant (p=0.099). Taken
together, these results indicate that the differences in the intracellular pattern may account
for the preserved NIR spectral profiles of the MTAB-TA GNR clusters. Further, we
examined the average diameter of extracellular GNR clusters in the TEM image with
ImageJ. Results indicated that the diameter of extracellular MTAB-TA GNR clusters was
larger than MTAB GNR clusters, 310 nm vs 165 nm, respectively (Figure 10 F). Based
on these finding, we tested if these differences in the intracellular MTAB and MTAB-TA
GNR clusters spectral profiles had any beneficial effect with nano-based biomedical
applications, specifically two-photon luminescence microscopy and photo-thermal
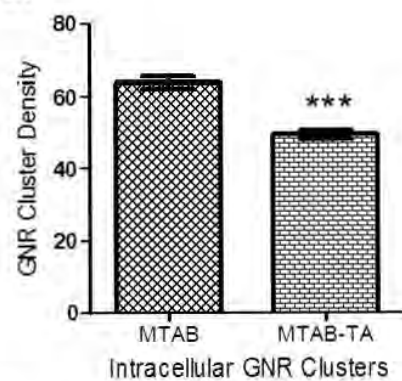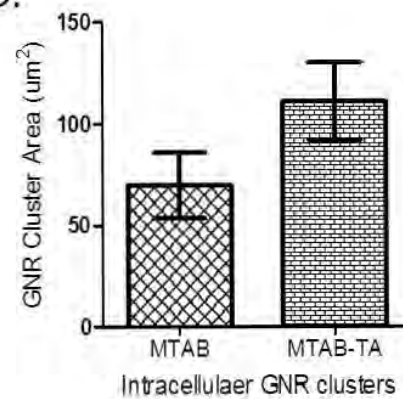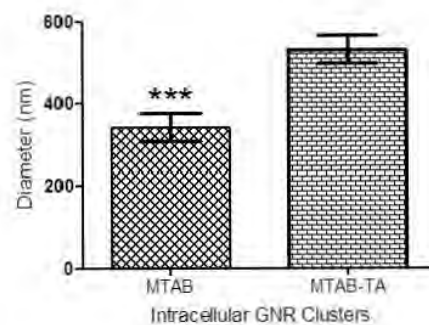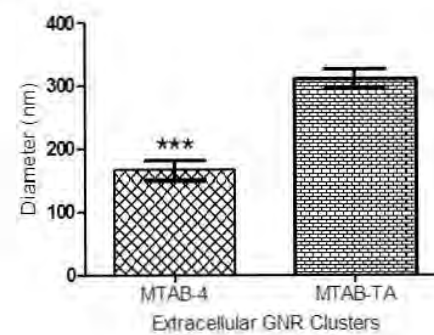cellular ablation.

Figure 10. Analysis of intracellular MTAB-TA GNR clusters.
Representative images of intracellular clusters in A549 cells after 24 h GNR exposure (20µg/ml) and clusters analysis using ImageJ software. A. MTAB B. MTAB-TA C. Average intracellular cluster density D. Average intracellular cluster area E. Average intracellular cluster diameter F. Average extracellular clusters diameter. Results demonstrated that MTAB-TA GNR clusters (n=24) are on average less densely packed (50% vs 64%) and have a large average diameter (534 nm vs 343 nm) compared to MTAB GNR groupings (n=28) in A549 cells. However, there was no statistically significant difference in the average intracellular cluster area, 70 ±16 µm^2 (MTAB) vs 111±19 µm^2 (MTAB-TA). The average diameter of extracellular MTAB-TA GNR clusters were larger than the average diameter of extracellular MTAB GNR clusters, 310 nm vs 165 nm, respectively. Statistical significance was determined using t-tests.

4.6 MTAB-TA GNRs exhibit superior two-photon luminescence image intensity
The use of GNRs has been described in a variety of bio-imaging modalities (Boca & Astilean, 2010; Eghtedari et al., 2007; von Maltzahn et al., 2009; Wang et al., 2005; T. Wang et al., 2013b). Of all these, nano-based bio-imaging two-photon luminescence imaging has been shown to provide the highest contrast and spatial resolution (Tong et al., 2009). Therefore, two-photon luminescence imaging was the focus of our bio-imaging studies. A strong two-photon luminescence intensity essential for bio-imaging as it allows for deeper imaging in tissues with less power.
Two-photon luminescence microscopy was used to capture 3-D images of A549 human lung cells that were exposed to GNRs (20 µg/mL) for 24 h. Next, we analyzed the intracellular MTAB and MTAB-TA GNR clusters with Fluoview software (Olympus, Pittsburgh, PA). The 3-D images were converted into 2-D images (Figure 11A-B) and the average intensity of MTAB and MTAB-TA GNR clusters was determined. Results demonstrated that intracellular MTAB-TA GNRs produced stronger two-photon luminescence intensity (798 ± 40.9 AU (161% of control)) when compared to intracellular MTAB (546 ± 25.1 AU (111% of control)). This indicated that the TA coating was able to reduce intracellular aggregation, protecting the GNRs key optical properties and NIR spectral signature, and in turn enhancing the GNRs bio-imaging capabilities.
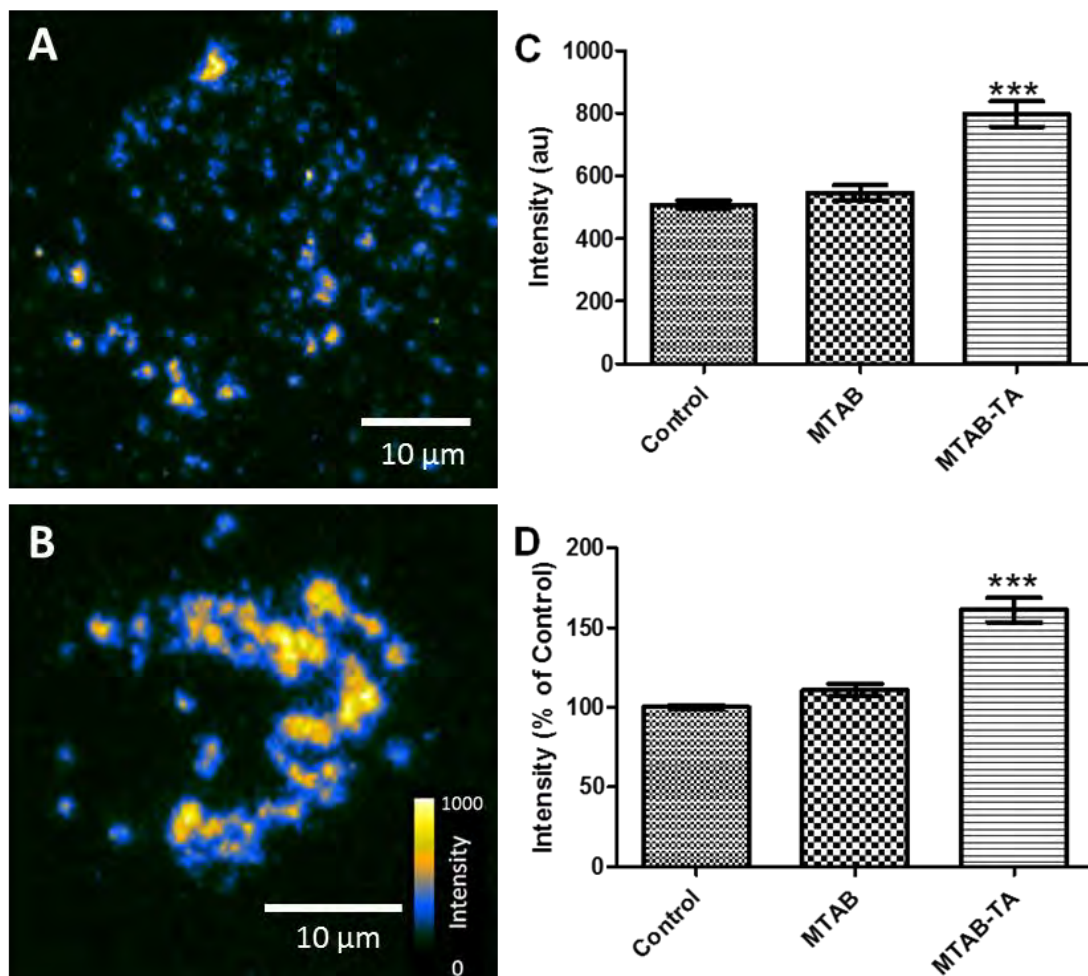
Figure 11. MTAB-TA GNRs display greater two-photon luminescence intensity. Representative images of A549 cells after GNR exposure (20µg/ml) for 24 h A. MTAB B. MTAB-TA GNRs. C. Average image intensity D. Average image intensity (% of control). Results demonstrated, on average, that the image intensity for cells with MTAB-TA GNR (798 ± 40.9 AU and 161% of control) is greater than cells with MTAB (546 ± 25.1 AU and 111% of control). Statistical significance was determined using t-tests.

4.7 MTAB-TA GNRs demonstrated higher efficiency for photo-thermal cellular ablation. The MTAB, MTAB-TA and silica GNRs all have spectral profiles that demonstrate longitudinal absorbance at approximately 810 nm. When these GNRs are exposed to corresponding 810 nm laser irradiation, the GNRs absorbs photons and this energy is converted to heat. This photothermal effect results in the GNRs becoming an extremely localized heat source that can be used to kill cancer cells via photo-thermal therapy (Cobley et al., 2011; Shanmugam et al., 2014; Zhang et al., 2012). The preserved spectral profile found in the intracellular MTAB-TA GNR suggests that they would be an excellent agent for photo-thermal therapy. To determine if the TA coating enhances the GNR photo-thermal properties *in vitro*, we used A549 adenocarcinomic human lung cells to evaluate the efficacy of MTAB and MTAB-TA GNR for photo-thermal cellular ablation. A549 human lung cells were exposed to the GNRs (20 µg/mL) for 24 h and

washed three times. Next, calcein AM (2 µM) and ethidium homodimer-1 (4 µM) was added to RPMI 1640 cell culture media without Phenol Red and incubated for 15 min. The cells were then irradiated with 60 sweeps of an 810nm 3W Ti-sapphire laser (30-75mW). Cellular ablation was measured at the 0, 1, 5, 10 min post irradiation time points. Results show that MTAB-TA is an effective photo-thermal therapeutic agent with cell viability decreasing as the laser power was increased (Figure 12). MTAB-TA GNR demonstrated the highest level of cell death and therefore the greatest efficacy for photo-thermal cellular ablation compared to MTAB and silica GNRs (Figure 13 & 26). Photo-thermal cellular ablation with silica GNRs resulted in non-uniform cell death in the irradiated field. This may be due to lower cellular uptake of silica GNRs (15%) compared to MTAB (40%) and MTAB-TA (39%) GNRs. Based on the cellular uptake results, the effective dose in the cell was approximately 3 µg/mL for the silica GNRs compared to approximately 8 µg/mL for MTAB and MTAB-TA GNRs. These photo-thermal cellular ablation results further confirms that the TA coating of GNRs preserves their optical properties and enhances their efficacy for photo-thermal applications.

	Pre	Exposure	1 Min	10Min
30mW				
45mW				
60mW				
75mW				

Laser Power

28
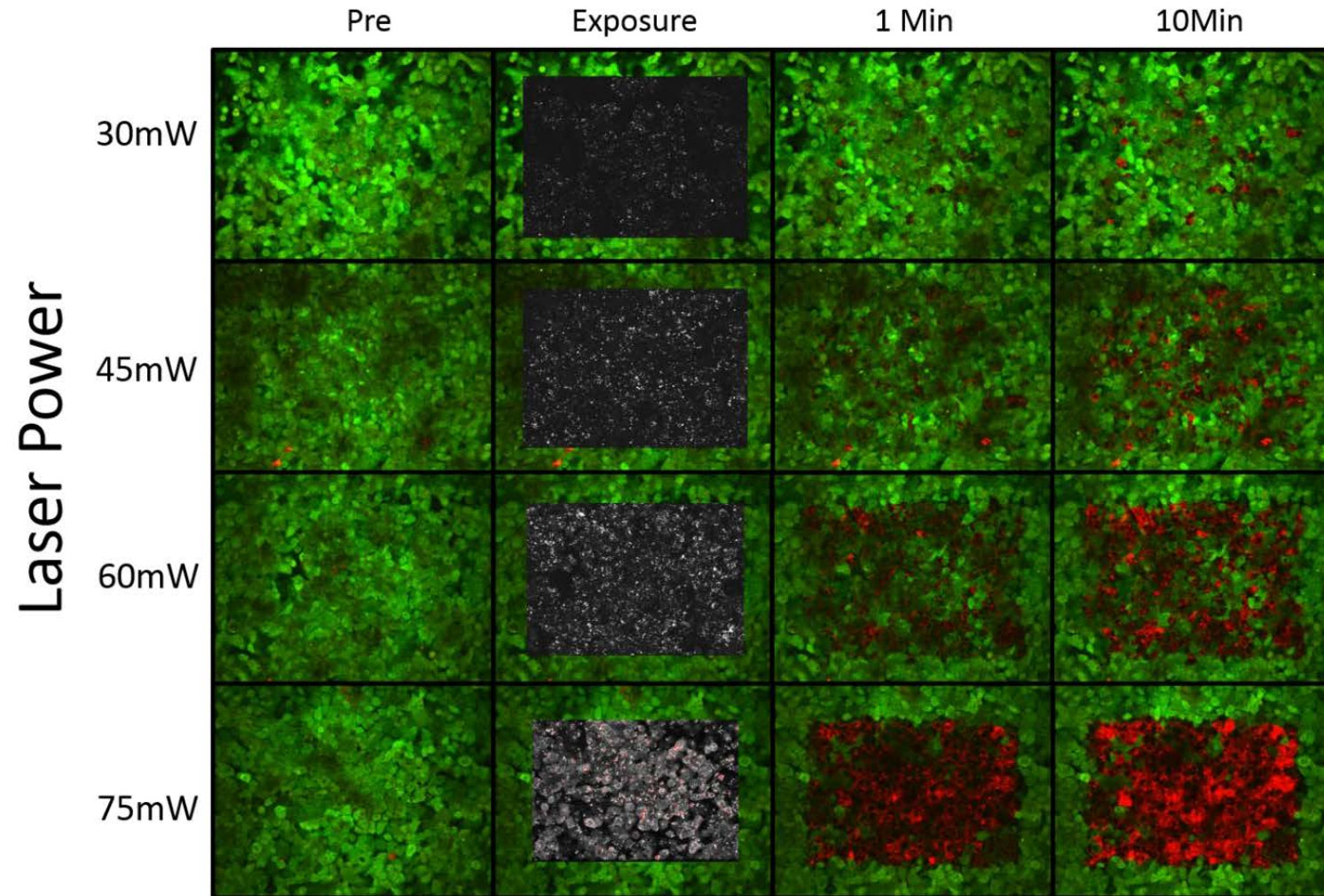
Figure 12. MTAB-TA GNR shows efficiency as agent for photo-thermal therapy.
Representative images of A549 cells after exposure to MTAB-TA GNRs (20µg/ml) for
24 h. Results show A549 cells before and after exposure to NIR laser irradiation. Results
show viability of MTAB-TA GNR treated cell decreasing as the laser power was
increased. Results demonstrate that MTAB-TA GNRs are an effective photo-thermal
therapeutic agent.

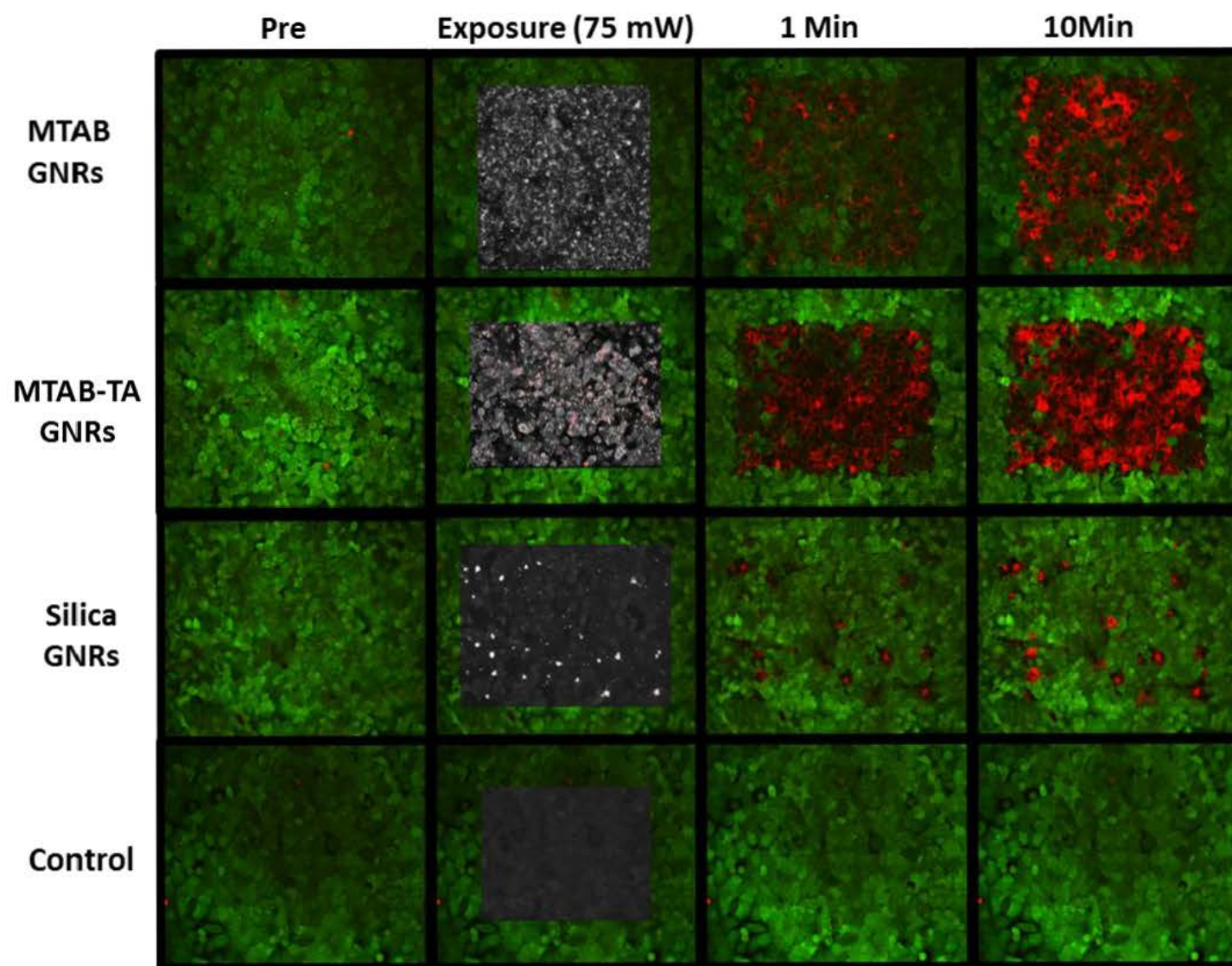|	Pre	Exposure (75 mW)	1 Min	10Min
MTAB GNRs				
MTAB-TA GNRs				
Silica GNRs				
Control				

Functionalized GNRs

Figure 13. Visual comparison of MTAB-TA GNRs efficiency for photo-thermal cellular ablation.
Representative images of A549 cells after exposure to GNRs (20 µg/ml) for 24 h. Results show A549 cells with MTAB, MTAB-TA, or silica GNRs before and after exposure to NIR laser irradiation. Results show that MTAB-TA has the greatest efficiency for photo-thermal cellular ablation as illustrated by the decrease in cell viability. Silica GNRs resulted in non-uniform killing of cells and GNR-free control showed no decrease in cell viability.
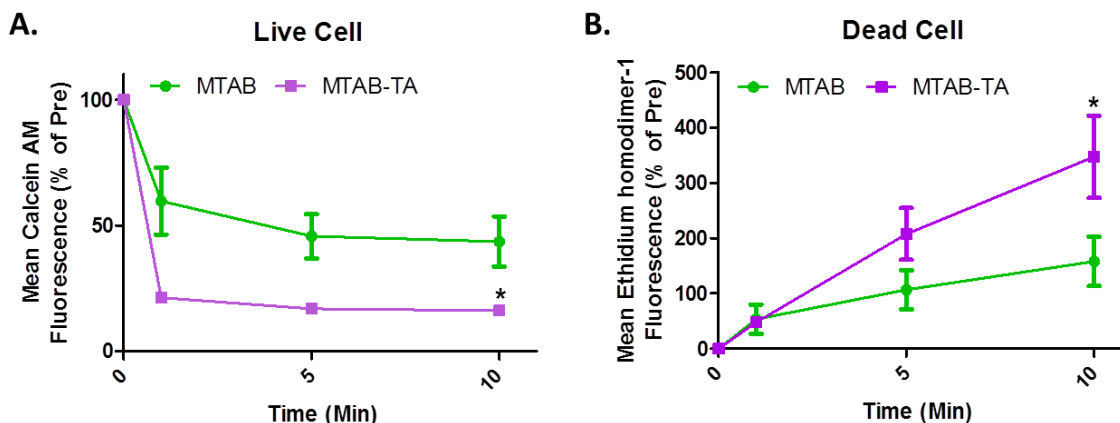

Figure 14. MTAB-TA GNRs demonstrate greatest efficiency for photo-thermal cellular ablation.
A549 human lung cells were exposed to GNRs (20 µg/ml) for 24 h and irradiated with 60 sweeps of an 810nm Ti-sapphire laser (75mW), cell viability was assessed using A. Mean Calcein AM fluorescence B. Mean ethidium homodimer-1flouescence. Results shows that photo-thermal cellular ablation with MTAB-TA GNRs results in both a significant decrease in mean Calcein AM fluorescence and a significant increase in mean ethidium homodimer-1 fluorescence. This indicates a significant decrease in cell viability and significant increase in cell death and demonstrates MTAB-TA GNRS superior photo-thermal cellular ablation properties. Statistical significance was determined using t-tests at 10 min post exposure.

5.0 CONCLUSIONS

In this study, the GNR surface chemistry was modified by replacing CTAB with MTAB and over-coating with TA. This created a novel GNR (MTAB-TA) that formed unique clusters, showed no decrease in cellular viability, no indication of cellular stress and no alteration of cell morphology, confirming its enhanced biocompatibility. Further, in the A549 human lung cancer cell line, MTAB-TA GNRs demonstrated a cellular uptake rate 26 times greater than the commonly used PEG GNRs and 2.5 times greater than silica coated GNRs (Figure 5). This high uptake rate would enable a lower effective diagnostic and therapeutic working concentration. The MTAB-TA GNRs displayed unique intracellular distribution patterns that not only preserved their NIR optical properties within the water but also enhanced their spectral intensity greater than 2.5 times that of uncoated GNRs. This finding is critical for bio-applications because it

allows for the use of minimally invasive NIR lasers, higher resolution imaging and more effective therapies. Finally, we demonstrated that the MTAB-TA GNRs had the greatest efficacy for photo-thermal cellular ablation compared to MTAB and silica GNRs (Figure 13 & 14). In conclusion, this study has identified the complete replacement of CTAB with MTAB and the use of TA to overcoat and create at soft shell around the GNR, reducing GNR aggregation, protecting and preserving the GNRs NIR optical properties intracellularly (Figure 15). Based on their biocompatible nature, high rate of *in vitro* cell internalization and low intracellular aggregation, MTAB-TA GNRs are prime candidates for use *in vivo* experimentation, nano-based bio-imaging and photo-thermal applications.
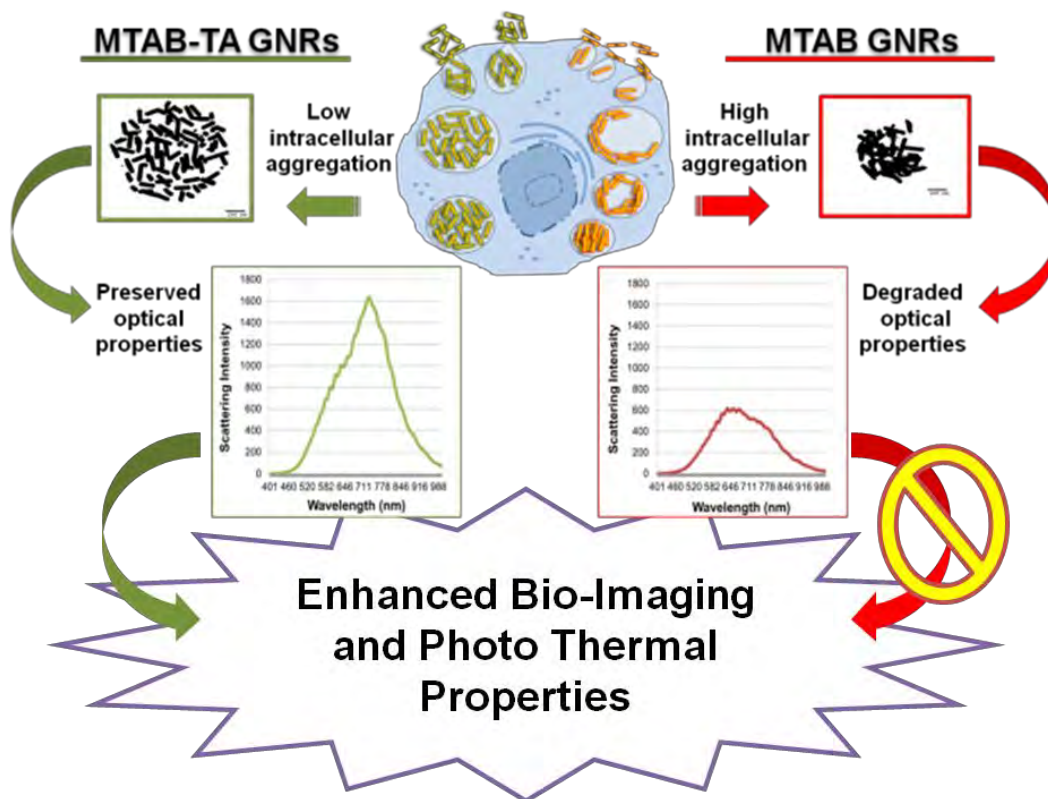
Figure 15. **MTAB-TA GNRs have enhanced bio-imaging and photo-thermal properties.** MTAB and MTAB-TA GNRs displayed high *in vitro* biocompatibility and cellular uptake. However, after internalization by A549 human lung cancer cells, the MTAB GNRs displayed high intracellular aggregation. This resulted in a degradation of the GNRs optical properties. On the contrary, TA coated MTAB GNRs (MTAB-TA) displayed low intracellular aggregation and preserved NIR optical properties. This results in greater two-photon image intensity and photo-thermal cellular ablation making them ideal nano-based bio-imaging and photo-thermal applications.

6.0 REFERENCES

Aaron, J., Travis, K., Harrison, N., & Sokolov, K. (2009). Dynamic imaging of molecular assemblies in live cells based on nanoparticle plasmon resonance coupling. Nano Lett, 9(10), 3612-3618. doi: 10.1021/nl9018275

Adlakha-Hutcheon, G., Khaydarov, R., Korenstein, R., Varma, R., Vaseashta, A., Stamm, H., & Abdel-Mottaleb, M. (2009). Nanomaterials, Nanotechnology. In I. Linkov & J. Steevens (Eds.), Nanomaterials: Risks and Benefits (pp. 195-207): Springer Netherlands.

Agarwal, A., Mackey, M. A., El-Sayed, M. A., & Bellamkonda, R. V. (2011). Remote triggered release of doxorubicin in tumors by synergistic application of thermosensitive liposomes and gold nanorods. ACS Nano, 5(6), 4919-4926. doi: 10.1021/nn201010q

Alkilany, A. M., & Murphy, C. J. (2010). Toxicity and cellular uptake of gold nanoparticles: what we have learned so far? Journal of Nanoparticle Research, 12(7), 2313-2333. doi: 10.1007/s11051-010-9911-8

Alkilany, A. M., Nagaria, P. K., Hexel, C. R., Shaw, T. J., Murphy, C. J., & Wyatt, M. D. (2009). Cellular uptake and cytotoxicity of gold nanorods: molecular origin of cytotoxicity and surface effects. Small, 5(6), 701-708. doi: 10.1002/smll.200801546

Barreto, J. A., O'Malley, W., Kubeil, M., Graham, B., Stephan, H., & Spiccia, L. (2011). Nanomaterials: applications in cancer imaging and therapy. Advanced Materials, 23(12), H18-H40.

Boca, S. C., & Astilean, S. (2010). Detoxification of gold nanorods by conjugation with thiolated poly(ethylene glycol) and their assessment as SERS-active carriers of Raman tags. Nanotechnology, 21(23), 235601. doi: 10.1088/0957-4484/21/23/235601

Bouhelier, A., Bachelot, R., Lerondel, G., Kostcheev, S., Royer, P., & Wiederrecht, G. P. (2005). Surface Plasmon Characteristics of Tunable Photoluminescence in Single Gold Nanorods. Physical Review Letters, 95(26), 267405.

Chithrani, B. D., Stewart, J., Allen, C., & Jaffray, D. A. (2009). Intracellular uptake, transport, and processing of nanostructures in cancer cells. Nanomedicine, 5(2), 118-127.

Choi, W. I., Sahu, A., Kim, Y. H., & Tae, G. (2012). Photothermal cancer therapy and imaging based on gold nanorods. Ann Biomed Eng, 40(2), 534-546. doi: 10.1007/s10439-011-0388-0

Cobley, C. M., Chen, J., Cho, E. C., Wang, L. V., & Xia, Y. (2011). Gold nanostructures: a class of multifunctional materials for biomedical applications. Chem Soc Rev, 40(1), 44-56. doi: 10.1039/b821763g

Debrosse, M. C., Comfort, K. K., Untener, E. A., Comfort, D. A., & Hussain, S. M. (2013). High aspect ratio gold nanorods displayed augmented cellular internalization and surface chemistry mediated cytotoxicity. Mater Sci Eng C Mater Biol Appl, 33(7), 4094-4100. doi: 10.1016/j.msec.2013.05.056

Eghtedari, M., Oraevsky, A., Copland, J. A., Kotov, N. A., Conjusteau, A., & Motamedi, M. (2007). High sensitivity of in vivo detection of gold nanorods using a laser optoacoustic imaging system. Nano Lett, 7(7), 1914-1918. doi: 10.1021/nl070557d

Ejima, H., Richardson, J. J., Liang, K., Best, J. P., van Koeverden, M. P., Such, G. K., . . . Caruso, F. (2013). One-step assembly of coordination complexes for versatile film and particle engineering. Science, 341(6142), 154-157. doi: 10.1126/science.1237265

Foster, K. A., Oster, C. G., Mayer, M. M., Avery, M. L., & Audus, K. L. (1998). Characterization of the A549 cell line as a type II pulmonary epithelial cell model for drug metabolism. Exp Cell Res, 243(2), 359-366. doi: 10.1006/excr.1998.4172

Grabinski, C., Schaeublin, N., Wijaya, A., D'Couto, H., Baxamusa, S. H., Hamad-Schifferli, K., & Hussain, S. M. (2011). Effect of gold nanorod surface chemistry on cellular response. ACS Nano, 5(4), 2870-2879. doi: 10.1021/nn103476x

Grabinski, C., Schlager, J., & Hussain, S. (2013). Hyperspectral microscopy for characterization of gold nanoparticles in biological media and cells for toxicity assessment. Methods Mol Biol, 1025, 167-178. doi: 10.1007/978-1-62703-462-3_13

Gui, C., & Cui, D. X. (2012). Functionalized gold nanorods for tumor imaging and targeted therapy. Cancer Biol Med, 9(4), 221-233. doi: 10.7497/j.issn.2095-3941.2012.04.002

Hauck, T. S., Ghazani, A. A., & Chan, W. C. (2008). Assessing the effect of surface chemistry on gold nanorod uptake, toxicity, and gene expression in mammalian cells. Small, 4(1), 153-159.

Hauck, T. S., Jennings, T. L., Yatsenko, T., Kumaradas, J. C., & Chan, W. C. (2008). Enhancing the toxicity of cancer chemotherapeutics with gold nanorod hyperthermia. Advanced Materials, 20(20), 3832-3838.

Huff, T. B., Hansen, M. N., Zhao, Y., Cheng, J.-X., & Wei, A. (2007). Controlling the Cellular Uptake of Gold Nanorods. Langmuir, 23(4), 1596-1599. doi: 10.1021/la062642r

Jain, P. K., Eustis, S., & El-Sayed, M. A. (2006). Plasmon coupling in nanorod assemblies: optical absorption, discrete dipole approximation simulation, and exciton-coupling model. J Phys Chem B, 110(37), 18243-18253. doi: 10.1021/jp063879z

Jana, N. R., Gearheart, L., & Murphy, C. J. (2001). Wet chemical synthesis of high aspect ratio cylindrical gold nanorods. The Journal of Physical Chemistry B, 105(19), 4065-4067.

Jelveh, S., & Chithrani, D. B. (2011). Gold nanostructures as a platform for combinational therapy in future cancer therapeutics. Cancers (Basel), 3(1), 1081-1110. doi: 10.3390/cancers3011081

Jun, T., Yong-Hua, L., Rong-Sheng, Z., Kai-Qun, L., Zhi-Guo, X., Zhao-Feng, L., . . . Hai, M. (2008). Effect of Aspect Ratio Distribution on Localized Surface Plasmon Resonance Extinction Spectrum of Gold Nanorods. Chinese Physics Letters, 25(12), 4459.

Kelly, K. L., Coronado, E., Zhao, L. L., & Schatz, G. C. (2003). The Optical Properties of Metal Nanoparticles: The Influence of Size, Shape, and Dielectric Environment. ChemInform, 34(16), no-no. doi: 10.1002/chin.200316243

Kuo, W. S., Chang, Y. T., Cho, K. C., Chiu, K. C., Lien, C. H., Yeh, C. S., & Chen, S. J. (2012). Gold nanomaterials conjugated with indocyanine green for dual-modality photodynamic and photothermal therapy. Biomaterials, 33(11), 3270-3278. doi: 10.1016/j.biomaterials.2012.01.035

Liang, A., Liu, Q., Wen, G., & Jiang, Z. (2012). The surface-plasmon-resonance effect of nanogold/silver and its analytical applications. TrAC Trends in Analytical Chemistry, 37(0), 32-47. doi: http://dx.doi.org/10.1016/j.trac.2012.03.015

Livak, K. J., & Schmittgen, T. D. (2001). Analysis of relative gene expression data using real-time quantitative PCR and the 2(-Delta Delta C(T)) Method. Methods, 25(4), 402-408. doi: 10.1006/meth.2001.1262

Mason, R. J., & Williams, M. C. (1980). Phospholipid composition and ultrastructure of A549 cells and other cultured pulmonary epithelial cells of presumed type II cell origin. Biochim Biophys Acta, 617(1), 36-50.

Mukhopadhyay, A., Grabinski, C., Afrooz, A. R., Saleh, N. B., & Hussain, S. (2012). Effect of gold nanosphere surface chemistry on protein adsorption and cell uptake in vitro. Appl Biochem Biotechnol, 167(2), 327-337. doi: 10.1007/s12010-012-9666-z

Nagesha, D., Laevsky, G. S., Lampton, P., Banyal, R., Warner, C., DiMarzio, C., & Sridhar, S. (2007). In vitro imaging of embryonic stem cells using multiphoton luminescence of gold nanoparticles. Int J Nanomedicine, 2(4), 813-819.

Nel, A. E., Mädler, L., Velegol, D., Xia, T., Hoek, E. M., Somasundaran, P., . . . Thompson, M. (2009). Understanding biophysicochemical interactions at the nano–bio interface. Nature materials, 8(7), 543-557.

Nikoobakht, B., & El-Sayed, M. A. (2003). Preparation and growth mechanism of gold nanorods (NRs) using seed-mediated growth method. Chemistry of Materials, 15(10), 1957-1962.

Pandey, S., Shah, R., Mewada, A., Thakur, M., Oza, G., & Sharon, M. (2013). Gold nanorods mediated controlled release of doxorubicin: nano-needles for efficient drug delivery. J Mater Sci Mater Med, 24(7), 1671-1681. doi: 10.1007/s10856-013-4915-4

Panyala, N. R., PeñaandMéndez, E. M., & Havel, J. (2009). Gold and nano-gold in medicine: overview, toxicology and perspectives. Journal of Applied Biomedicine, 2009.

Park, K. (2006). Synthesis, Characterization, and Self –Assembly of Size Tunable Gold Nanorods (Doctor of Philosophy Dissertation), Georgia Institute of Technology. Retrieved from http://hdl.handle.net/1853/14035

Park, K., & Vaia, R. A. (2008). Synthesis of Complex Au/Ag Nanorods by Controlled Overgrowth. Advanced Materials, 20(20), 3882-3886. doi: 10.1002/adma.200800613

Pissuwan, D., Valenzuela, S., & Cortie, M. B. (2008). Prospects for gold nanorod particles in diagnostic and therapeutic applications. Biotechnol Genet Eng Rev, 25, 93-112.

Qiu, Y., Liu, Y., Wang, L., Xu, L., Bai, R., Ji, Y., . . . Chen, C. (2010). Surface chemistry and aspect ratio mediated cellular uptake of Au nanorods. Biomaterials. doi: 10.1016/j.biomaterials.2010.06.051

Schneider, C. A., Rasband, W. S., & Eliceiri, K. W. (2012). NIH Image to ImageJ: 25 years of image analysis. Nat Meth, 9(7), 671-675.

Shanmugam, V., Selvakumar, S., & Yeh, C. S. (2014). Near-infrared light-responsive nanomaterials in cancer therapeutics. Chem Soc Rev, 43(17), 6254-6287. doi: 10.1039/c4cs00011k

Sosa, I. O., Noguez, C., & Barrera, R. G. (2003). Optical Properties of Metal Nanoparticles with Arbitrary Shapes. The Journal of Physical Chemistry B, 107(26), 6269-6275. doi: 10.1021/jp0274076

Stacy, B., Comfort, K., Comfort, D., & Hussain, S. (2013). In Vitro Identification of Gold Nanorods through Hyperspectral Imaging. Plasmonics, 8(2), 1235-1240. doi: 10.1007/s11468-013-9538-6

Sun, Y., & Xia, Y. (2002). Shape-Controlled Synthesis of Gold and Silver Nanoparticles. Science, 298(5601), 2176-2179. doi: 10.1126/science.1077229

Takahashi, H., Niidome, Y., Niidome, T., Kaneko, K., Kawasaki, H., & Yamada, S. (2005). Modification of Gold Nanorods Using Phosphatidylcholine to Reduce Cytotoxicity. Langmuir, 22(1), 2-5. doi: 10.1021/la0520029

Tong, L., Wei, Q., Wei, A., & Cheng, J. X. (2009). Gold nanorods as contrast agents for biological imaging: optical properties, surface conjugation and photothermal effects. Photochem Photobiol, 85(1), 21-32. doi: 10.1111/j.1751-1097.2008.00507.x

Uboldi, C., Bonacchi, D., Lorenzi, G., Hermanns, M. I., Pohl, C., Baldi, G., . . . Kirkpatrick, C. J. (2009). Gold nanoparticles induce cytotoxicity in the alveolar type-II cell lines A549 and NCIH441. Part Fibre Toxicol, 6, 18. doi: 10.1186/1743-8977-6-18

Untener, E. A., Comfort, K. K., Maurer, E. I., Grabinski, C. M., Comfort, D. A., & Hussain, S. M. (2013). Tannic acid coated gold nanorods demonstrate a distinctive form of endosomal uptake and unique distribution within cells. ACS Appl Mater Interfaces, 5(17), 8366-8373. doi: 10.1021/am402848q

Van Buren, J. P., & Robinson, W. B. (1969). Formation of complexes between protein and tannic acid. Journal of Agricultural and Food Chemistry, 17(4), 772-777.

Vigderman, L., Khanal, B. P., & Zubarev, E. R. (2012a). Functional gold nanorods: synthesis, self-assembly, and sensing applications. Adv Mater, 24(36), 4811-4841, 5014. doi: 10.1002/adma.201201690

Vigderman, L., Manna, P., & Zubarev, E. R. (2012b). Quantitative Replacement of Cetyl Trimethylammonium Bromide by Cationic Thiol Ligands on the Surface of Gold Nanorods and Their Extremely Large Uptake by Cancer Cells. Angewandte Chemie International Edition, 51(3), 636-641. doi: 10.1002/anie.201107304

von Maltzahn, G., Park, J. H., Agrawal, A., Bandaru, N. K., Das, S. K., Sailor, M. J., & Bhatia, S. N. (2009). Computationally guided photothermal tumor therapy using long-circulating gold nanorod antennas. Cancer Res, 69(9), 3892-3900. doi: 10.1158/0008-5472.CAN-08-4242

Wagner, R. C. (1976). The effect of tannic acid on electron images of capillary endothelial cell membranes. Journal of ultrastructure research, 57(2), 132-139.

Walkey, C. D., & Chan, W. C. W. (2012). Understanding and controlling the interaction of nanomaterials with proteins in a physiological environment. Chem Soc Rev, 41(7), 2780-2799. doi: 10.1039/C1CS15233E

Walkey, C. D., Olsen, J. B., Song, F., Liu, R., Guo, H., Olsen, D. W. H., Chan, W. C. W. (2014). Protein Corona Fingerprinting Predicts the Cellular Interaction of Gold and Silver Nanoparticles. ACS Nano, 8(3), 2439-2455. doi: 10.1021/nn406018q

Wang, C., Chen, J., Talavage, T., & Irudayaraj, J. (2009). Gold Nanorod/Fe3O4 Nanoparticle "Nano-Pearl-Necklaces" for Simultaneous Targeting, Dual-Mode Imaging, and Photothermal Ablation of Cancer Cells. Angew Chem Int Ed Engl, 121(15), 2797-2801. doi: 10.1002/ange.200805282

Wang, H., Huff, T. B., Zweifel, D. A., He, W., Low, P. S., Wei, A., & Cheng, J. X. (2005). In vitro and in vivo two-photon luminescence imaging of single gold nanorods. Proc Natl Acad Sci U S A, 102(44), 15752-15756. doi: 10.1073/pnas.0504892102

Wang, L., Li, J., Pan, J., Jiang, X., Ji, Y., Li, Y., . . . Chen, C. (2013a). Revealing the binding structure of the protein corona on gold nanorods using synchrotron radiation-based techniques: understanding the reduced damage in cell membranes. J Am Chem Soc, 135(46), 17359-17368. doi: 10.1021/ja406924v

Wang, L., Liu, Y., Li, W., Jiang, X., Ji, Y., Wu, X., . . . Chen, C. (2011). Selective targeting of gold nanorods at the mitochondria of cancer cells: implications for cancer therapy. Nano Lett, 11(2), 772-780. doi: 10.1021/nl103992v

Wang, T., Halaney, D., Ho, D., Feldman, M. D., & Milner, T. E. (2013b). Two-photon luminescence properties of gold nanorods. Biomed Opt Express, 4(4), 584-595. doi: 10.1364/BOE.4.000584

Weissleder, R. (2001). A clearer vision for in vivo imaging. Nat Biotech, 19(4), 316-317.

Yang, H. W., Liu, H. L., Li, M. L., Hsi, I. W., Fan, C. T., Huang, C. Y., . . . Wei, K. C. (2013).
Magnetic gold-nanorod/ PNIPAAmMA nanoparticles for dual magnetic resonance and
photoacoustic imaging and targeted photothermal therapy. Biomaterials, 34(22), 5651-5660.
doi: 10.1016/j.biomaterials.2013.03.085

Zhang, W., Ji, Y., Wu, X., & Xu, H. (2013a). Trafficking of gold nanorods in breast cancer cells:
uptake, lysosome maturation, and elimination. ACS Appl Mater Interfaces, 5(19), 9856-
9865. doi: 10.1021/am4033857

Zhang, Y., Qian, J., Wang, D., Wang, Y., & He, S. (2013b). Multifunctional gold nanorods with
ultrahigh stability and tunability for in vivo fluorescence imaging, SERS detection, and
photodynamic therapy. Angew Chem Int Ed Engl, 52(4), 1148-1151. doi:
10.1002/anie.201207909

Zhang, Z., Wang, J., & Chen, C. (2013c). Gold nanorods based platforms for light-mediated
theranostics. Theranostics, 3(3), 223-238. doi: 10.7150/thno.5409

Zhang, Z., Wang, L., Wang, J., Jiang, X., Li, X., Hu, Z., . . . Chen, C. (2012). Mesoporous silica-
coated gold nanorods as a light-mediated multifunctional theranostic platform for cancer
treatment. Adv Mater, 24(11), 1418-1423. doi: 10.1002/adma.201104714

LIST OF ACRONYMS

ATCC	American Type Culture Collection
AR	Aspect Ratio
CTAB	Cetyl trimethylammonium Bromide
DLS	Dynamic Light Scattering
FBS	Fetal Bovine Serum
GNMs	Gold Nanomaterials
GNRs	Gold Nanorods
HIS	Hyperspectral Imaging
ICP-MS	Inductively Coupled Plasma Mass Spectrometry
LCDC	Live Cell Dead Cell
MTAB	11-mercaptohexadecyl trimethylammonium Bromide
MTS	(3-(4,5-dimethylthiazol-2-yl)-5-(3-carboxymethoxyphenyl)-2-(4-sulfophenyl)-2H-tetrazolium)
NIR	Near-Infrared
NM	Nanomaterial
PBS	Phosphate Buffered Saline
PEG	Polyethylene glycol
ROS	Oxygen Species
SPR	Surface Plasmon Resonance
TA	Tannic Acid
TEM	Transmission Electron Microscopy
UV-Vis	Ultra-Violet Visible Spectroscopy